Measurement of Dust Cloud Characteristics in Industrial Plants[1]

Final Technical Report

F. Hauert A. Vogl

January 1995

[1]Number: PL 910695

Contents

List of Figures

1 Project Objectives

In industrial plants, where combustible dusts or dust containing goods are produced, processed or stored, dust explosions may be expected. Assuming dust/air–mixtures with concentrations above the Lower–Explosion–Limit (LEL) and below the Upper–Explosion–Limit (UEL) various modes of ignition (electric sparks, hot surfaces...) can cause an explosion [3, 6].

The selection and optimum adaptation of safety measures to operational conditions based on risk analysis represents a main area of problems in industrial safety.
Previous investigations have shown, that real dust clouds can be described by the following parameters, which can be determined by measurements:

Flow field $\longrightarrow$ velocity and local and temporal turbulence intensity
Dust distribution $\longrightarrow$ local and temporal dust concentration

In the present context turbulence may be described as a state of rapid, more or less random, movement of the particles of a dust cloud relative to each other in three dimensions [7].

Two kinds of turbulence, differing by their origin, have to be considered. The initial turbulence is generated by the industrial process in which the dust cloud is formed, whether a cyclone, a pneumatic transport pipe, or a mill. The second kind of turbulence is generated by the explosion itself by expansion–induced flow of unburned dust cloud ahead of the propagating flame front [7]. In this report we will consider only the initial turbulence.

Various investigations showed [1, 4, 11, 13, 16] that in addition to the specific dust characteristics and the thermodynamic parameters (e.g. pressure, temperature) the particle size and concentration distribution of the dust/air mixture as well as its turbulence, have an important effect on the turbulent flame velocity and consequently on the explosion violence.
As shown by various authors the initial turbulence will effect mainly the pressure rise, that is the gradient of pressure vs. time. Nevertheless, there is an influence upon the maximum pressure in a dust explosion, which will decrease slightly [6].

However, there is only little information on these parameters available with respect to the formation of dust clouds during processing. Therefore, the objective of the present research project is to characterize real dust clouds in industrial plants using special measuring techniques.

2 Physical characterization of dust/air-mixtures

Dust is generated during various technical or industrial processes as a product, by–product or as waste stream. Normally, dust is defined as a disperse solid matter with a particle size below 500 μm. Mixtures consisting of particles with a size less than 100 μm are described as fine dust. The morphology of dust particles is extraordinarily diverse. There are spherical as well as none spherical shapes with a smooth, porous or fibrous surface. Examples of various dusts are given in fig. 2, which were taken with a Scanning–Electron–Microscope. Generally, the size of the dust particles varies within one single mixture (fig. 1).

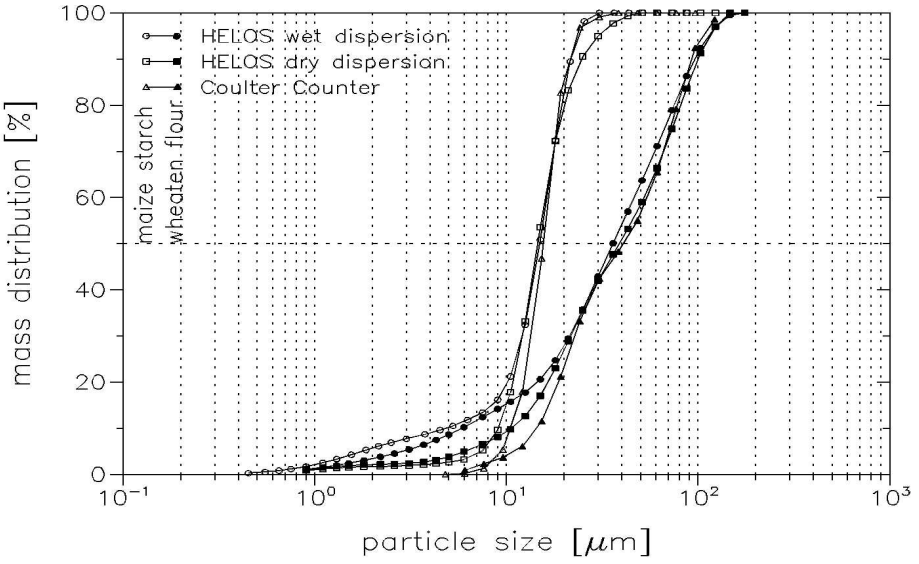

Figure 1: Particle size distribution of maize starch and wheaten flour. The measurements were carried out with three different laser scattering systems.

The motion of the dispersed dust causes local and temporal changes in concentration. The segregation is caused by the sedimentation of the particles at different rates according to their weight, size and shape under the influence of gravity. Because of the frictional resistance, the free-falling dust particle reaches its final velocity v_E quite quickly. Considering the different forces effecting a single particle (law of Stokes, gravity, buoyancy) we yield

$$v_E = \frac{2}{9} \cdot \frac{x_{St}^2 \cdot g \cdot (\rho_p - \rho_f)}{\eta_f}$$

$$x_{pm} = x_{st} \cdot \Psi^{-\frac{3}{4}}$$

x_{St}	[m]	Stoke - diameter
η_f	[kg/ms]	dynamic viscosity (at 20 ^{o}C = $1.8{\cdot}10^{-5}\,\frac{kg}{m\,s}$)
v_E	[m/s]	sedimentation velocity
g	[m/s^2]	gravitational acceleration
ρ_p	[kg/m^3]	particle density
ρ_f	[kg/m^3]	air density (at 20 ^{o}C = 1.29 $\frac{kg}{m^3}$)
x_{pm}	[m]	mean particle diameter
Ψ		form factor (sphericity)

$\Psi \approx 0.8$ for round particle
$\Psi \approx 0.3 - 0.6$ for fibrous and angular particle surface

In practice it has to be expected, that the dust particles are subject to movement by the air stream caused by the type of plant or process. This may reduce the effect of gravity or may even neutralize it (e.g. pneumatic conveying, fluidized bed drier).

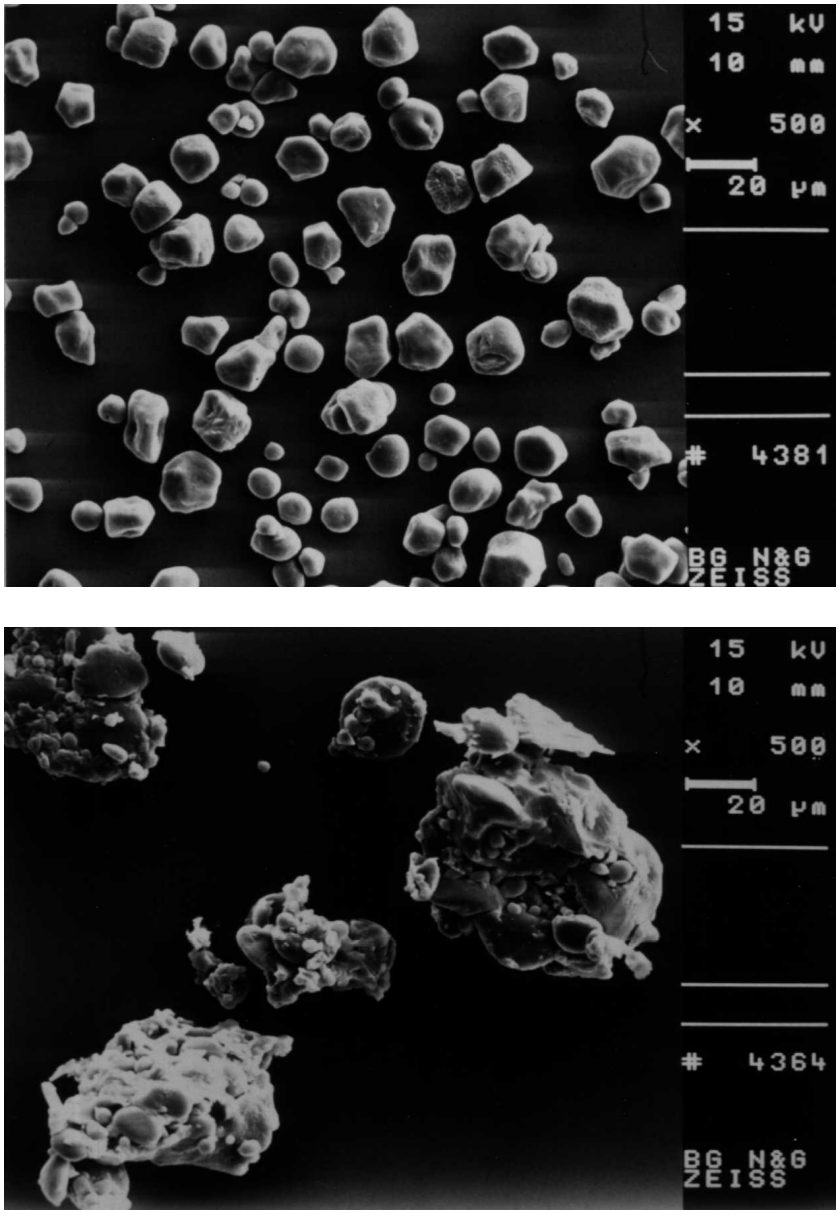

Figure 2: Photos of dust taken with a Scanning–Electron–Microscope (500 times magnification). The upper picture shows maize starch the lower wheaten flour.

2.1 Dust types

For the main investigations we used three different dust types, where the median–value is given in brackets (fig. 1).

1. maize starch (15 μm)
2. wheaten flour (35 μm)
3. Titanium dioxide TiO_2 (1 μm).

TiO_2 was only used in the 12 m^3–silo and the 1 m^3–vessel to validate the results of the food dusts. Additional, barley was used in the discharge trench and crushing mill, maisarin was used in the discharge trench and maizegluten and tapioca in the ship hull and finally technocel was used in the bed drier.

3 Description of the measuring technique

3.1 Measurement of the flow field

Laser-Doppler-Anemometry (LDA) is popularly used to measure eddy flows in various fields. By using a sufficiently fast data collection it is possible to describe the turbulent structure of the flow. By means of the LDA it is only possible to measure the velocity of particles, but not of the air flow. Therefore, tracer particles like TiO_2 are often used to make an air flow measurable for the Laser-Doppler-Anemometry. The influence of the tracer particle size upon the flow information can be estimated for spherical particles according to the Basset-Boussinesq-Oseen equation [10, 15].

Our measurements of the velocity and the turbulence in the vessel were carried out with the aid of a portable and compact Laser–Doppler–Anemometry–System, where the probe is connected with the flow analyser by an optical fiber (DANTEC, Flowlite)[17].

3.1.1 Principle of LDA

The basic operating principle of the Laser–Doppler–Anemometry is described as follows [14, 5]:

A laser beam is split and the two resulting beams are focused to cross each other at a given angle, and therefore, they are coherent to each other at the point of their intersection. If two coherent laser beams intersect, they interfere in the volume of intersection, forming interference fringes. If a particle traverses this volume, and a photo detector is arranged to receive light scattered from a source in this

volume, the received light will consist of two components, one corresponding to each of the beams. Both components will have a Doppler shift due to the velocity of the particle. However, the shift is also dependent upon the direction of the light beam. Since the two beams are at an angle, the two components of scattered light have different Doppler shifts. At the surface of the photo detector, therefore, the two light components interfere, resulting in a pulsating light intensity. With the proportionality between velocity and Doppler frequency, it is possible to calculate the resulting velocity of the particle.

To overcome the problem that a positive and a negative velocity of the same magnitude will result in the same Doppler shift, the frequency of one of the two crossing beams is shifted by a Bragg cell (40 MHz). Consequently, the fringe pattern is no longer stationary but moves at constant velocity.

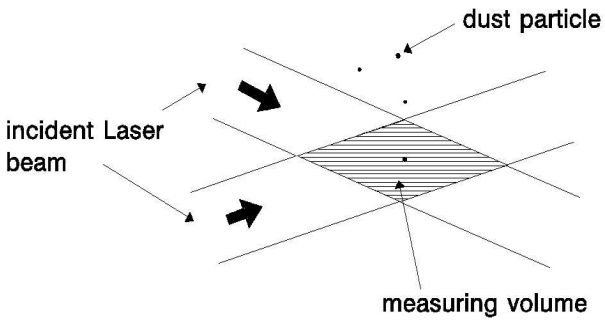

Figure 3: Principle of Laser-Doppler-Anmometry to determine the velocity of a particle. The measuring volume consists of fringes due to the interference of the two laser beams.

The probe of the LDA has a length of 100 mm and a diameter of 16 mm, where the front lens has a focal length of 50 mm. The advantage of this focal length is, that the motion of the particle is not disturbed by the measurement probe itself and on the other hand the penetrating depth is not reduced due to light scattering by the dust particles.

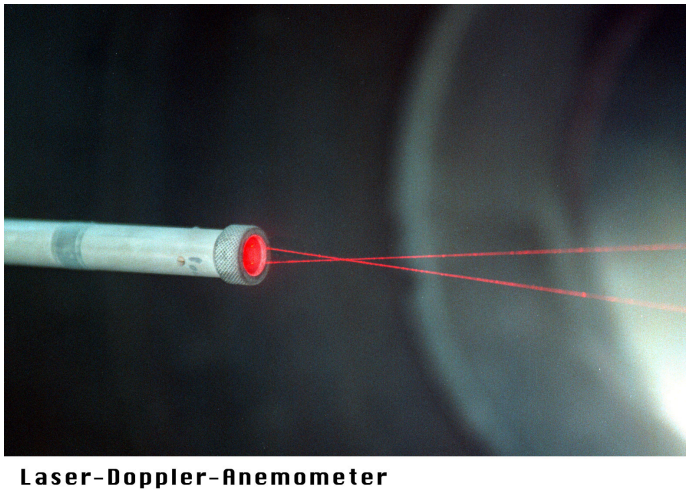

Figure 4: Photograph of the LDA-probe mounted in a metal tube. [Photo: Maag]

Since the probe was installed in a metal tube, which has a length of 1.5 m it is possible to vary the position of the intersection volume in radial direction. This allows us also to change the orientation of the intersection volume to measure the horizontal and the vertical velocity component of the particles, respectively. To protect the lens, a small window was located at the end of the tube. Furthermore, a nozzle was mounted, allowing to clean the window with air–pressure. Before starting every measurement in the 12 m^3–silo, the window was cleaned with a short gust of air.

3.1.2 Evaluation of the data

The analysis process of the data consists of two major methods: The removal of erroneous data points and the calculation of the mean velocity and RMS turbulence velocity using a time averaging procedure.

The erroneous data points resulting from noise in the signal or from the simultaneous measurement of more than one particle have a great influence on the calculation of the velocity parameters. To detect the erroneous data points every single point was compared with its two neighbors (one both sides). If the difference is larger than an empirical determined factor, the point was deleted. From tests with various factors this value was optimized.

For a time interval $\tau = t' - t$ centered around a single data point the mean velocity $\bar{u}$ and the RMS–turbulence velocity RMS are calculated according to

$$\bar{u} = \frac{1}{\tau} \int_t^{t'} u(t)\, dt \approx \frac{1}{N} \sum_{i=1}^{N} u_i \tag{1}$$

$$RMS = \sqrt{\frac{1}{\tau} \int_t^{t'} (u(t) - \bar{u})^2\, dt} \approx \sqrt{\frac{\sum_i (u_i - \bar{u})^2}{N}} \tag{2}$$

where N is the total number of measurements and u_i is the velocity of "i" particle.

The calculations are performed for each data point within the time interval resulting in two data sets for each interval. The size of the time interval is essential in this procedure, and therefore, it was adjusted empirically in several tests.

3.2 Measurement of the dust concentration

For the characterization of dust clouds the local measurement of the dust concentration is of great importance additional to the knowledge of the flow ratios. Because

such a measuring instrument is not placed on the market, the *FSA* did its own development.

3.2.1 Measuring principle

The dust concentration was determined by measuring the light transmission using opto-electronic techniques.

The measuring principle (fig. 5) is based on the attenuation of the intensity of a light beam by absorption and dispersion penetrating a cloud with solid particles [21]. The ratio between the resulting and the initial intensity is defined as transmission [12]. "Lambert-Beer's law" describes the relation between the transmission and the dust concentration c according to the following equation:

$$I = I_o \cdot e^{-\epsilon \cdot c \cdot l} \tag{3}$$

I_o = initial intensity
I = resulting intensity of the light beam
ϵ = Coefficient of extinction (a specific constant for the dust type and the appliance)
l = distance
c = dust concentration

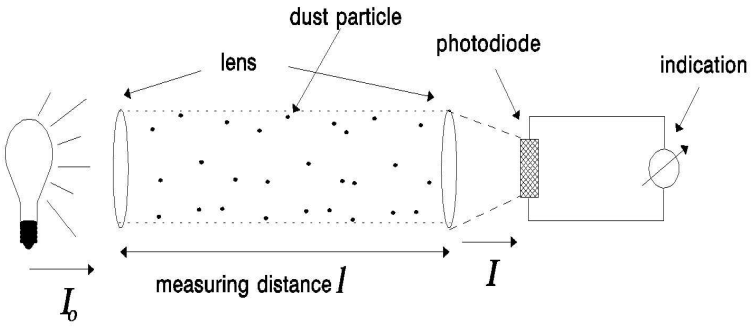

Figure 5: Schematic diagram of the dust concentration measuring principle. Due to the absorption and light scattering at the dust particles, the intensity of the light beam is attenuated.

Fig. 6 shows the schematic diagram of the developed probe of the dust concentration measuring instrument with the optic and the cleaning system.

For the light source (rectangular pulses) an efficient GaAs-Luminescent-diode with its maximum spectral sensitivity at 950 nm is used [2]. Consequently, a photo diode of the same spectral sensitivity was used for receiving [20]. The clock frequency

was chosen in a way that even rapid changes or momentary peak values of the dust concentration up to about 3 kHz are exactly reproduced.

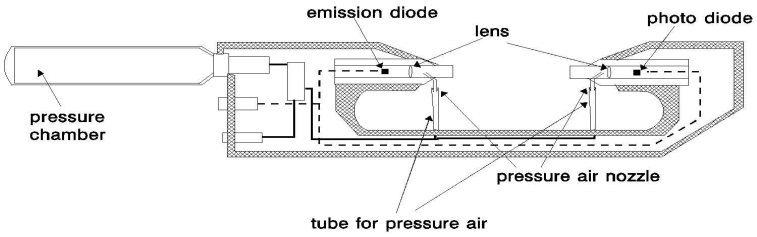

Figure 6: Schematic diagram of the probe of the dust concentration measuring instrument.

The measured signal received from the photo diode is converted to a DC signal and either displayed directly or stored in a PC.

The power pack, an electronic card, control elements and a digital display are installed in a portable casing. Additionally, the sensors (Fig. 7) are equipped with a cleaning system using compressed air. The optimization of this cleaning device, that is, minimizing the influence on the results, was carried out in the labs of *FSA*.

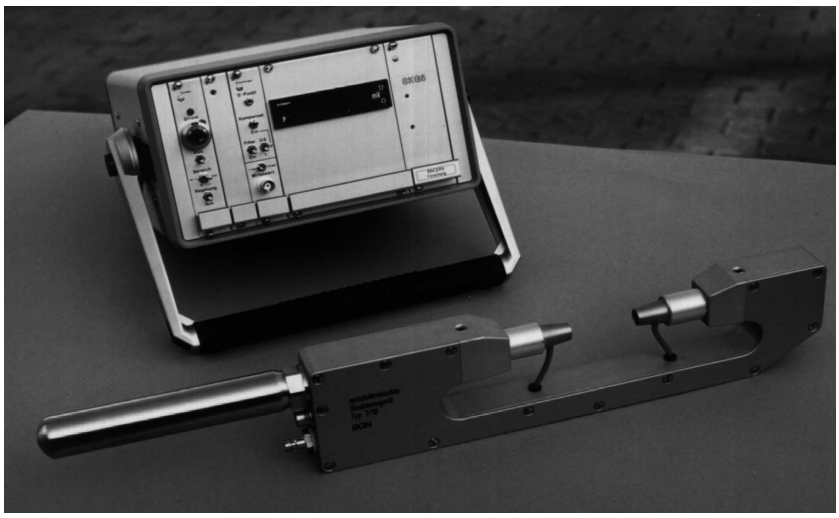

Figure 7: Dust concentration measuring probe.

The system is calibrated by changing the quantity of dust in a suspension systematically, that is, the Coefficient of Extinction ϵ can be achieved from Lambert–Beer's Law Eq. (3) (see fig. 8).

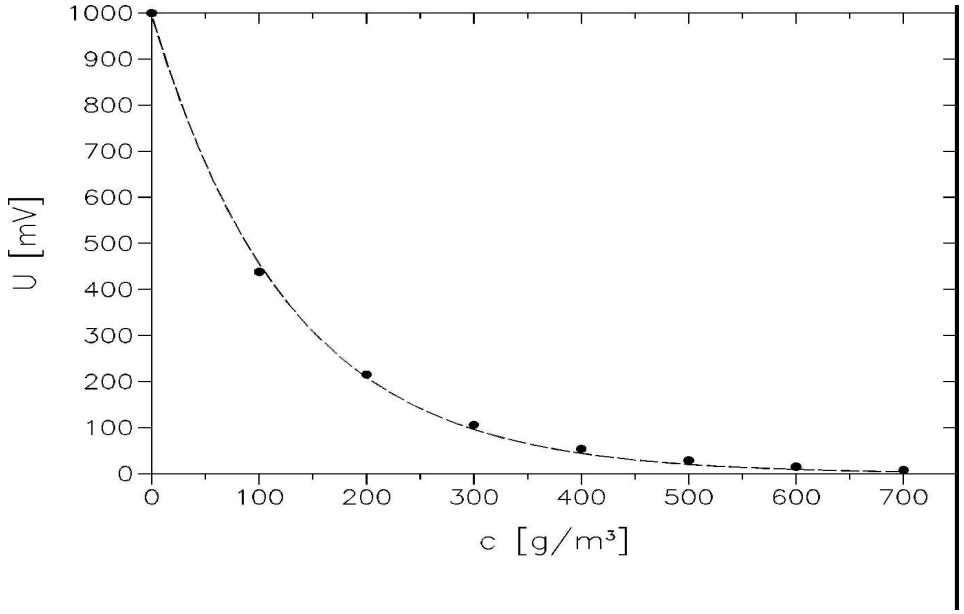

Figure 8: Calibration curve of the dust concentration measuring system for maize starch. The measuring distance was l= 10 cm.

3.2.2 Measuring errors

In this research project measurements have to be carried out with very difficult environmental conditions (for example dust concentration measurements in the fluidized bed drier), and therefore, additional equipment was necessary.

Calibrating the system carefully and taking the application limits (for example ambient temperature) into account [20] changes of the particle size distribution during the measurement and soiling of the sensor optics remain as relevant errors in measurement.

The sensitive components of the sensors are extraordinarily protected against pollution, due to their location within the sensor casing.

Errors in measurements occur, if the grain size range within the dust cloud changes due to sedimentation.

If fine dusts with a median value $M < 100\mu$m are tested, as well as in the presence of very turbulent flow ratios (for example pneumatic flight conveying) the influence of the errors mentioned above are quite small, which is, from the explosion-technical view, of great interest.

4 Measurements at a 12 m^3–Silo

4.1 Experimental Approach

To characterize dust clouds in process industries, a small silo has been constructed, which can be fed with dust mechanically and pneumatically. The product can be fed into the vessel either vertically (i.e. axial) or tangentially. A rotary air lock at the silo outlet allows the recycling of the dust into the conveying system, so that circulation is possible.

The silo has a volume of V = 12 m^3 with a height/diameter ratio of H/D = 3.5. Fig. 9 shows the general structure. The diameter of the silo is 1.6 m.

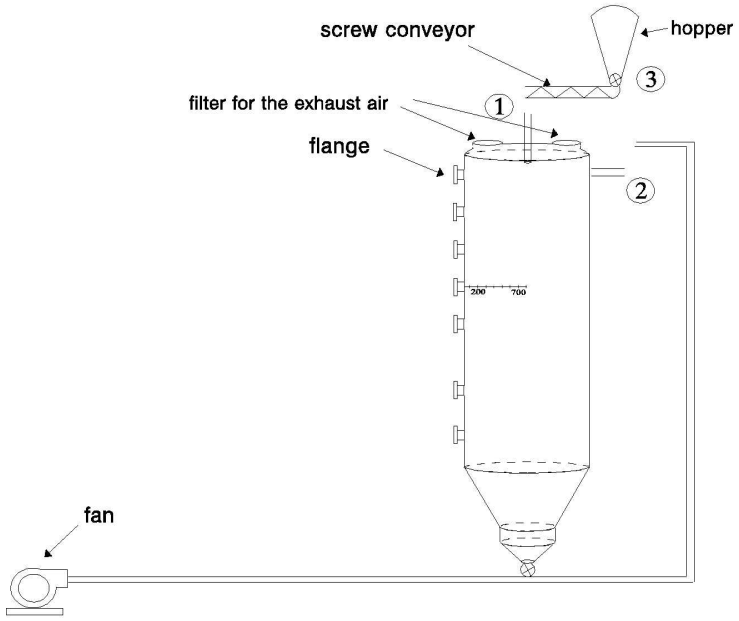

Figure 9: Schematic picture of the experimental 12 m^3–silo. Three possibilities to fill the silo: (1) pneumatical vertical or axial, (2) pneumatical tangential and (3) mechanical with a screw conveyor after a hopper.

The capacity of the pneumatic system (3 t/h) and the screw conveyor was adapted to the size of the silo.

The maximum air stream of the pneumatic conveying system is about 8 m^3/min. With a diameter of the conveying pipe of 75 mm and a conveying velocity of 30 m/s the conveying stream can be fed at most with 7-8 kg/m^3 fine dust, for example maize starch. Filling the silo pneumatically the exhaust air leaves the silo through 3 filters mounted at the top of the silo. Each of the filter has a cross-section of 0.78 m^2. It is possible to clean the filter pneumatically, too.

The cylindrical vessel wall is equipped with various flanges for the measuring technique in a systematic order, so that measurements at different levels of the vessel are possible. Fig. 10 shows the silo with its 7 different positions at different height. If the inlet is mounted exactly, rotary symmetry is assumed.

At one level the silo is equipped with three flanges with an angle of 120^o. While fig. 10 shows the arrangement of the flanges and the measuring positions, Fig. 11 shows the set up in practice.

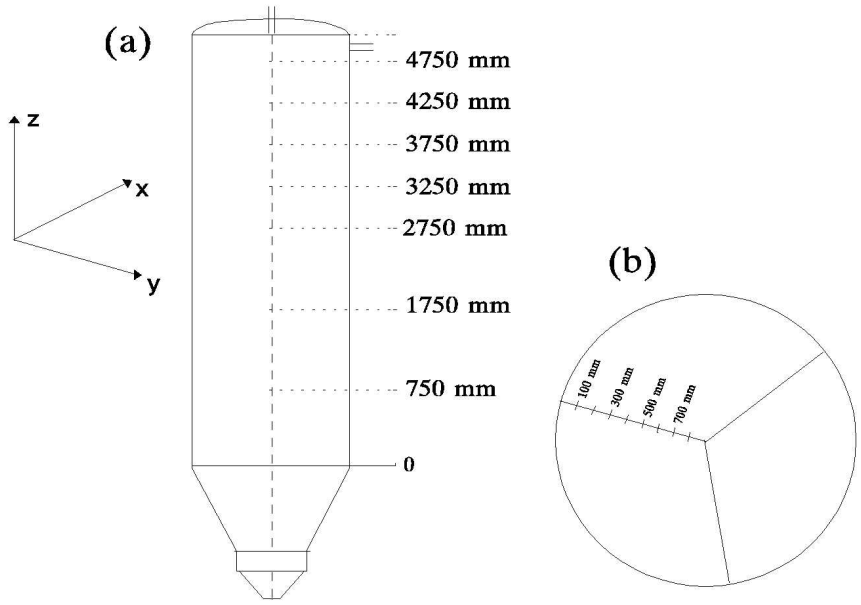

Figure 10: (a) Various positions at the silo for the measuring probes. (b) shows the x-y plane of the silo and the eight positions in radial direction at which the measurements were carried out.

For simultaneous measurements of the dust concentration and to reduce the scan time, altogether eight measuring instruments were constructed, so that measurements at various positions can be carried out simultaneously. As shown in fig. 12 two probes, which are supplied with nozzles to clean the lenses with compressed air, are mounted at the vessel.

For the measurements the following boundary conditions can be varied:

- the way of feeding:
  - pneumatical axially
  - pneumatical tangentially
  - mechanical by the means of a screw conveyor

Figure 11: Photograph of the 12 m^3–silo fed vertically pneumatically.

- type of dust:
  - maize starch
  - wheaten flour (type 550)
  - Titanium dioxide
- feeding rate ξ:
  - 1 kg/m^3
  - 3 kg/m^3
  - 7 kg/m^3

Due to the measuring conditions the duration of a single measurement is limited. Because of the pollution of the lens–system of the probe, the signal-to-noise ratio

Figure 12: Dust concentration measurement probes mounted at the 12 m^3–silo.

becomes worse and no further measurement is possible. To avoid this problem, several short measurements were carried out consecutively with intermediate cleaning of the lenses.

When a stationary flow is provided, it enables us to measure the velocity at arbitrary times, if the steady state is reached. We averaged 10 single measurements (each about 5000 data points) at every position to the resulting velocity and turbulence.

4.2 Results

4.2.1 Flow field

Axial feeding

The Laser Doppler Anemometry produces a sequence of non-equidistant velocity measurements, i.e. the velocity of the different particles is plotted versus the arrival time (fig. 13).

Fig. 13 shows the RMS turbulence velocity in z-direction (axial) and in the x-y plane (tangential) for a dust feeding rate of 7 kg/m^3. These measurements were conducted at the level 3750 mm.

The tangential velocity components are constant within their margin of error. The tangential components of the turbulence show approximately the same behavior as the axial; however, the amount seems to be lower (fig. 13).

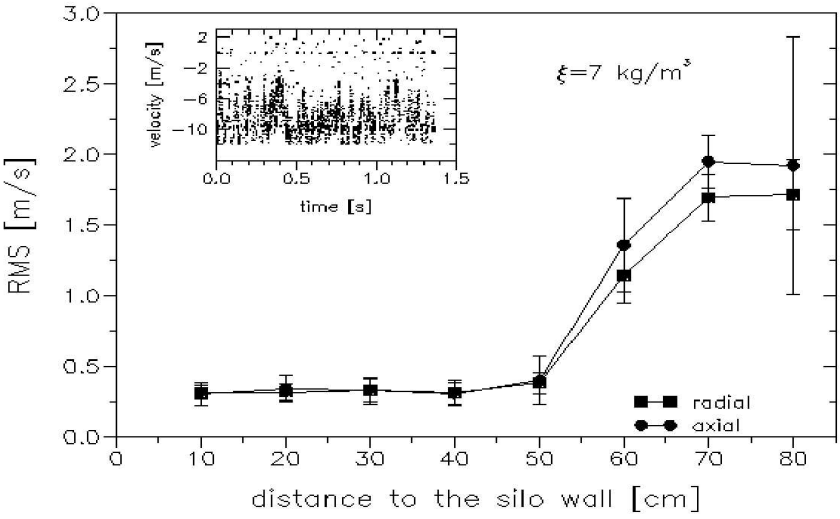

Figure 13: Comparison of the tangential and the axial component of the RMS turbulence velocity measured at a height of 3750 mm (feeding rate ξ= 7 kg/m^3). The inset shows a typical time history of the velocity. Every point characterizes the velocity of one single particle.

Fig. 14 compares the mean velocity and the RMS turbulence velocity using various feeding rates 1, 3 and 7 kg/m^3 for the axial component. It can be seen that the mean velocities are nearly independent on the dust feeding rate. The RMS turbulence velocity fluctuates a little more from each other, however, no systematic deviation was found within the error limits of each single test.

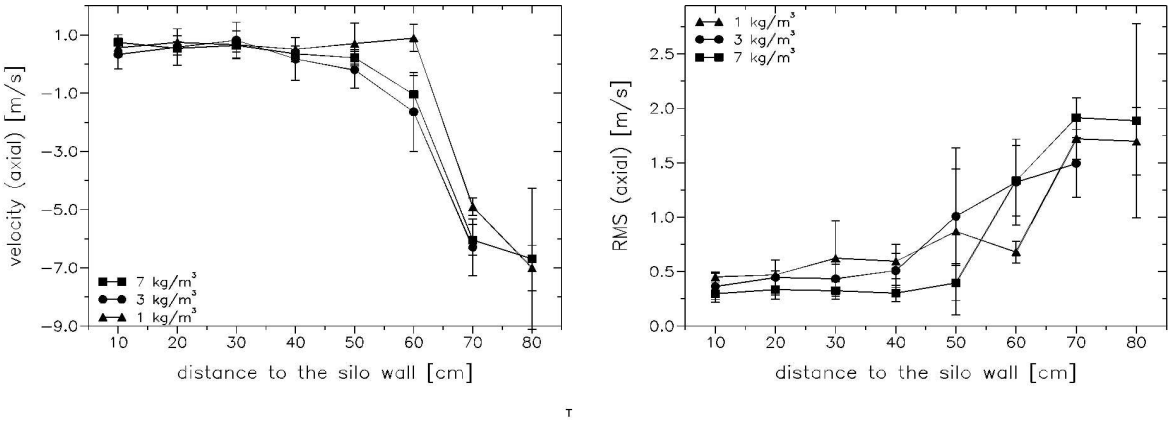

Figure 14: Influence of the various feeding rates upon the axial component of the velocity (left side) and the RMS turbulence velocity (right side) measured at a height of 3750 mm using maize starch.

The influence of the dust type is shown in fig. 15 for the velocity and the RMS turbulence velocity. The diagram shows, that only directly in the beam (i.e. 70 cm and 80 cm distance to the silo wall) the measured parameters vary for the three types of dust.

It must be emphasized, that the measured RMS turbulence intensity is below 1 m/s. Only directly in the beam the RMS-value increases up to 2.5 m/s.

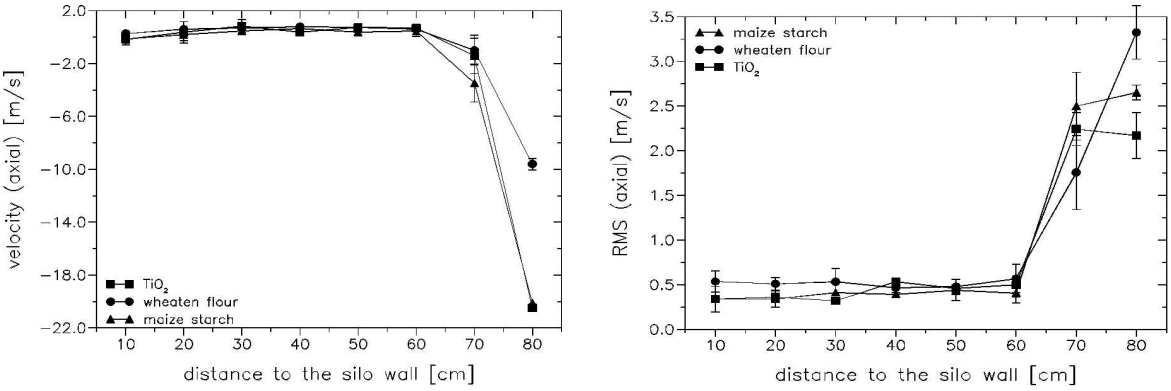

Figure 15: Effect of the various dust types upon the axial component of the velocity (left side) and the RMS turbulence velocity (right side) measured at a height of 4750 mm (feeding rate ξ= 1 kg/m^3).

Fig. 16 gives a survey of the velocity and turbulence in the whole silo.

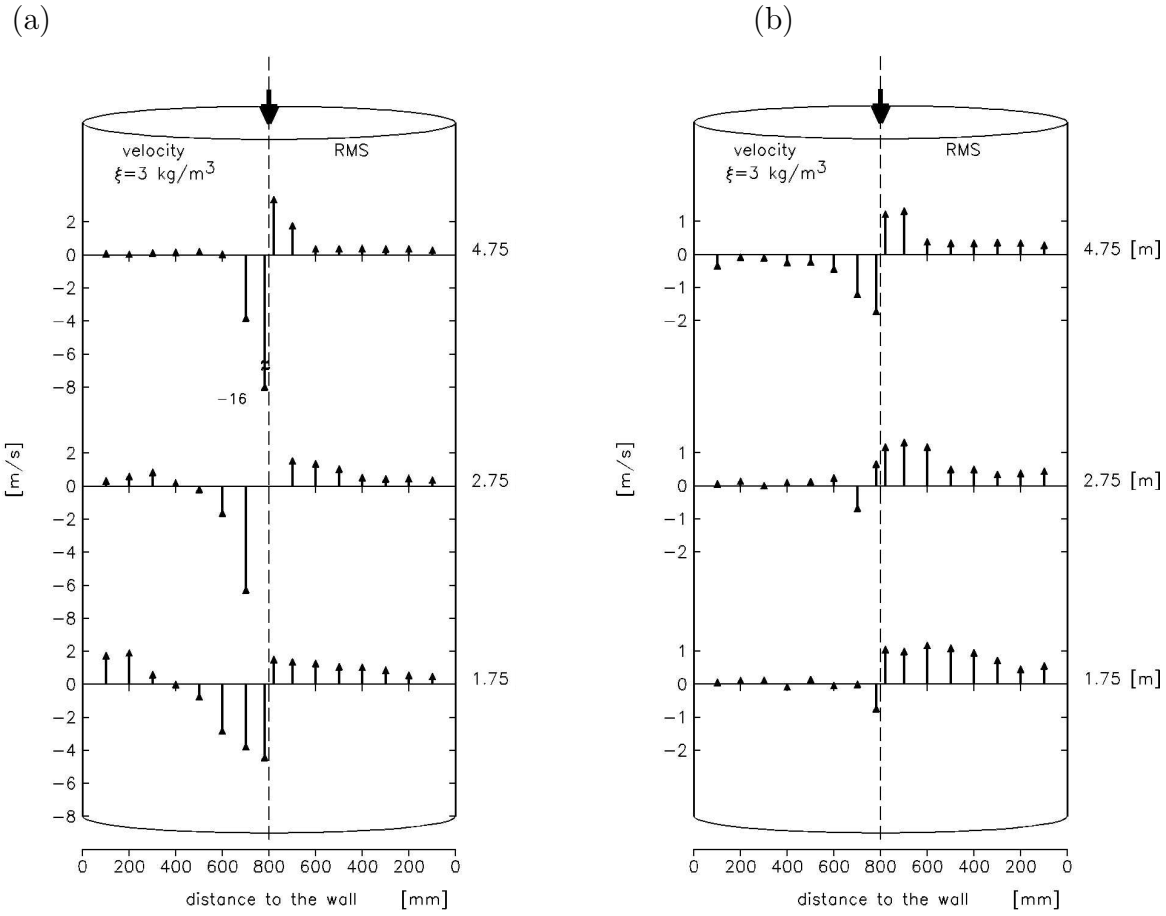

Figure 16: Survey of the results using axial feeding with maize starch for the velocity and RMS turbulence velocity (ξ=3 kg/m^3). (a) Measured velocity (left side) and turbulence (right side) for the axial component along the z–direction. (b) same parameters as in a) but measured component tangential to the radius (i.e. x-y-plane).

Tangential feeding

The measurement of the velocity and the turbulence filling the silo tangential yields the following results using cylindrical coordinates (r, φ, z). The rotary symmetry, which was measured at the height 3750 mm is valid in this case. We measured in each case both components (z-direction and tangential to the radius $\varphi = 0$) of the velocity and of the RMS turbulence velocity.

Fig. 17 shows the influence of the various feeding rates. The corresponding RMS turbulence velocities are quite small across the cross-section.

As expected the velocity of the tangential component decreases from the silo wall to the center as shown in fig. 18. The corresponding RMS turbulence velocity is small and nearly constant.

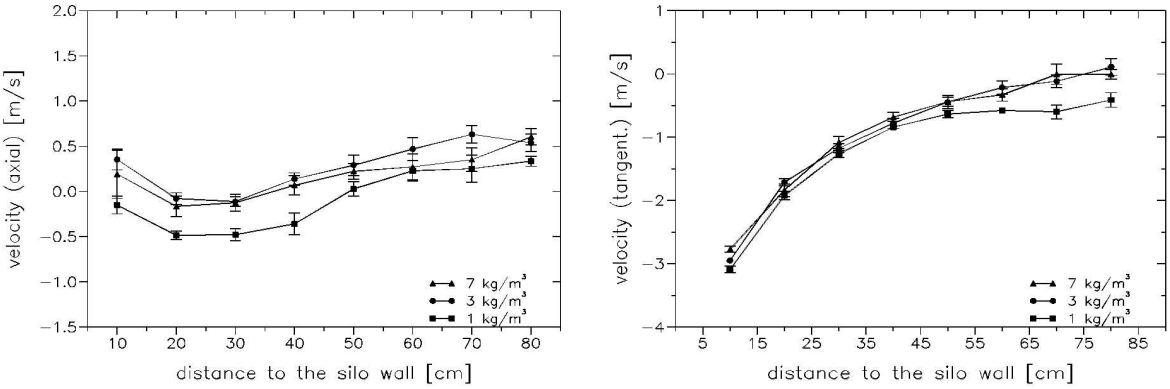

Figure 17: Influence of the various feeding rates upon the axial (left side) component and the tangential (right side) component of the velocity measured at a height of 3750 mm filling the silo tangential with maize starch.

Considering the component in z-direction it can be seen a reversal of the velocity near the center of the silo in all planes. The reason of that phenomena is the displace of the exhaust air, which leaves the silo centrally through the filter. The RMS turbulence velocity shows only small variation.

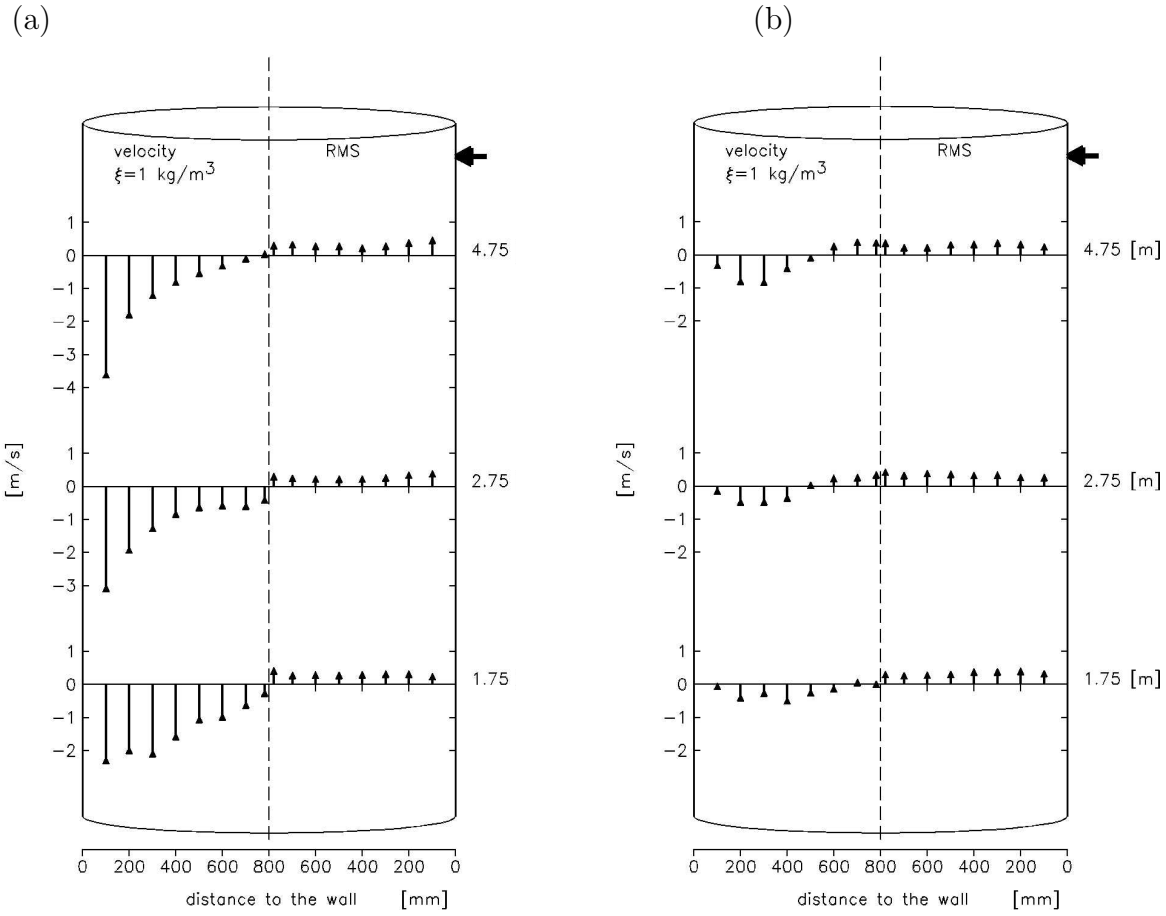

Figure 18: Survey of the results using tangential feeding with maize starch for the velocity and RMS turbulence velocity (ξ=1 kg/m^3). (a) Measured velocity (left side) and turbulence (right side) for the component tangential to the radius (i.e. x-y-plane). (b) axial component, i.e. along z–direction.

Mechanical feeding

According to fig. 9 the silo was also fed mechanically by the means of a screw conveyor, where the hopper was filled pneumatically. As expected the velocity is quite small (fig. 19) due to gravity forces, and also the RMS turbulence velocity is below 0.3 m/s. The data rate during the measurements shows a strong dependence upon the moisture of the dust.

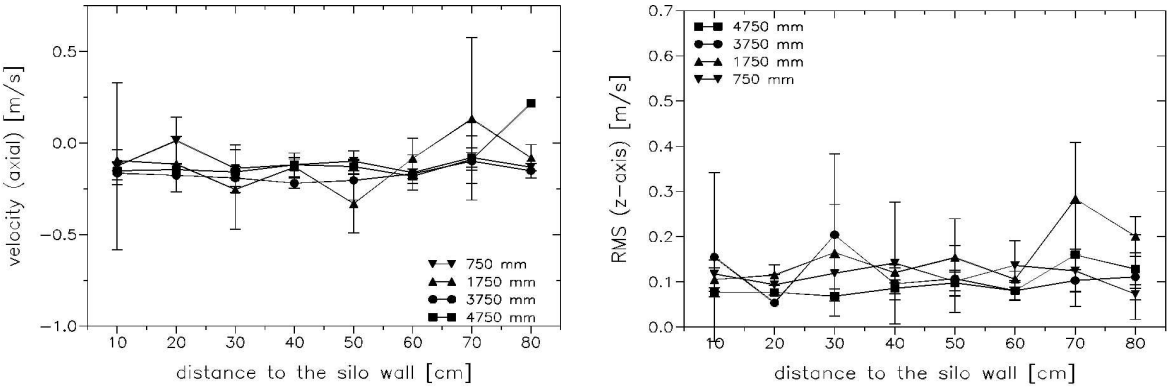

Figure 19: Measured velocity and RMS turbulence velocity (axial component) at different levels filling the silo mechanical by the means of a screw conveyor after a hopper.

4.2.2 Dust distribution

Axial feeding

The measurement of the local and temporal dust concentration was first conducted at the empty vessel, that is, no dust in the conical outlet. The dust was discharged vertically with a conveying velocity of v_F=27 m/s (constant for all tests).

Five measuring probes were mounted vertically with a distance of 1 m to each other. Additional, two measuring probes were mounted at the height 1750 mm.

Fig. 20 shows a typical time history of the dust concentration at two different positions (750 mm and 4750 mm). The data were averaged over time intervals, where the length τ of the interval was determined empirically. The corresponding standard deviation σ ($\bar{c} \pm \sigma$) was calculated by evaluating N various time intervals. The total measuring time was varied between 5 and 30 min.

In table 1 the average values of the measured dust concentrations at various heights of the silo are given for a feeding rate of 3 kg/m^3. In this case the distance to the silo wall was d = 400 mm. Although different time intervals between two cleaning cycles were evaluated, the average dust concentration shows only poor variation. This indicates stable experimental conditions.

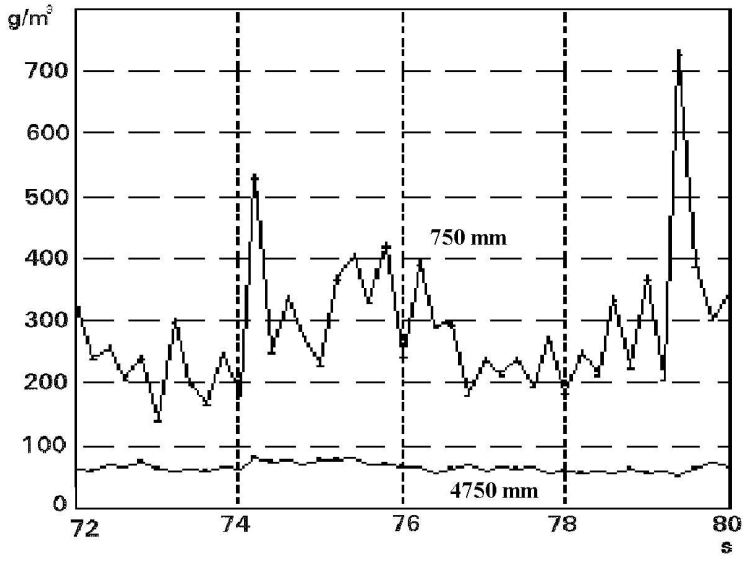

Figure 20: Example for the measured time history of the dust concentration at the position 750 mm and 4750 mm; distance to the silo wall d = 400 mm, ξ=3 kg/m^3.

Table 1: Dust concentration measured in the 12 m^3-vessel feeding pneumatically vertically; feeding rate $\xi = 3$ kg/m^3, maize starch, distance to the wall $d = 400$ mm. The concentration is averaged during the time interval τ. $\bar{c}$ denotes the mean value of the average dust concentration during all time intervals.

position h d	750 mm 400 mm	1750 mm 400 mm	1750 mm 400 mm	2750 mm 400 mm	3750 mm 400 mm	4750 mm 400 mm
time interval $[s]$	c $[\frac{g}{m^3}]$	c $[\frac{g}{m^3}]$	c $[\frac{g}{m^3}]$	c $[\frac{g}{m^3}]$	c $[\frac{g}{m^3}]$	c $[\frac{g}{m^3}]$
72 – 80	285	244	340	201	85	64
93 – 100	258	243	301	183	93	69
133 – 140	256	289	307	188	107	68
567 – 575	276	256	295	186	99	54
719 – 726	276	290	230	180	97	69
1113 – 1121	242	323	298	245	107	57
1133 – 1141	251	342	289	202	87	73
1335 – 1342	244	341	278	206	89	58
$\bar{c}$	261	291	292	199	96	64
σ	16.1	41.2	31	21	8.5	6.9

Especially in the area close to the main dust beam and at the bottom of the silo, where the dust was dispersed the dust concentration varies about the mean concentration resulting in sharp peaks. Fig. 20 shows two signals one from the lower (height $h = 750$ mm) and the second from the upper area of the silo ($h = 4750$ mm).

Normally, rotary symmetry can be assumed for the axial filling. A few experiments were carried out to check this assumption. Fig. 21 shows the results for vertical pneumatical filling with wheaten flour (feeding rate 7 $\frac{kg}{m^3}$). The measuring probes were arranged with an angle of 120^o around the silo according to fig. 10(b). It can be seen that the rotary symmetry is not satisfied in this case. The reason for this phenomenon is, that the inlet was not mounted exactly parallel to the z–axis of the silo, and therefore, the dust stream is not straight.

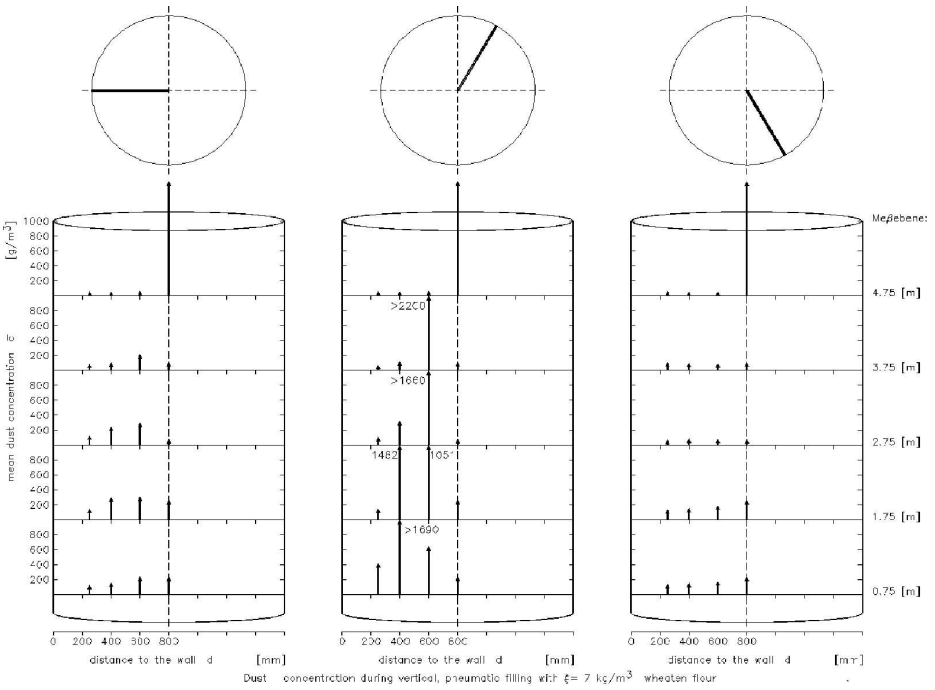

Figure 21: Dust concentration in the vertical pneumatical fed 12 m^3–silo. The feeding rate was ξ=7 $\frac{kg}{m^3}$ using maize starch. The three pictures show the different measuring positions, which were arranged around the silo with 120^o.

In a second step the measuring probes were mounted at various distances d to the silo wall: $d = 250$, 400, 600 and 800 mm. The mean dust concentration depending upon the various dust feeding rates (ξ= 1, 3 and 7 kg/m^3) is shown in fig. 22 and 23 as a function of the height h. Independent on the amount of dust, the same tendencies can be noticed:

- if the probe is closer than 400 mm to the wall the dust concentration decreases with increasing height

- close to the center of the silo (d= 600 mm – 800 mm) the measuring position is located in the dust beam itself with increasing height

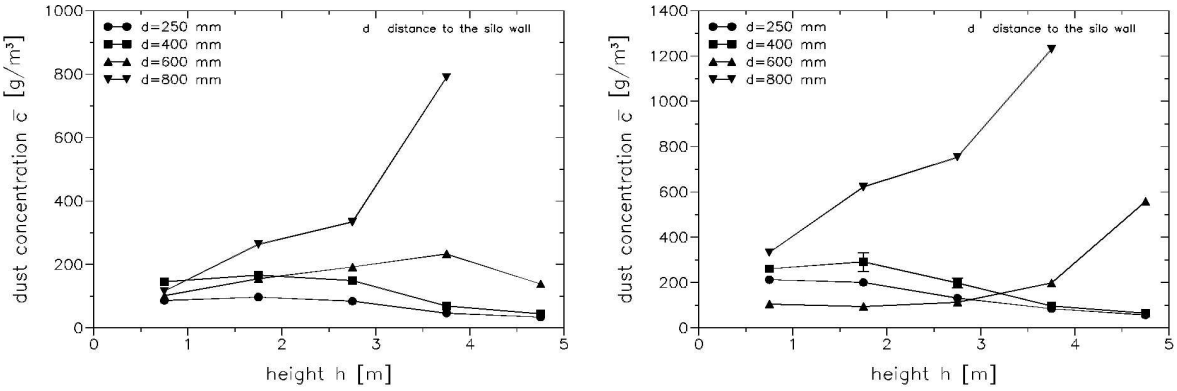

Figure 22: Mean dust concentration versus the height h at the silo fed vertical with a feeding rate of ξ=1 kg/m^3 (left picture) and ξ=3 kg/m^3 (right picture) using maize starch.

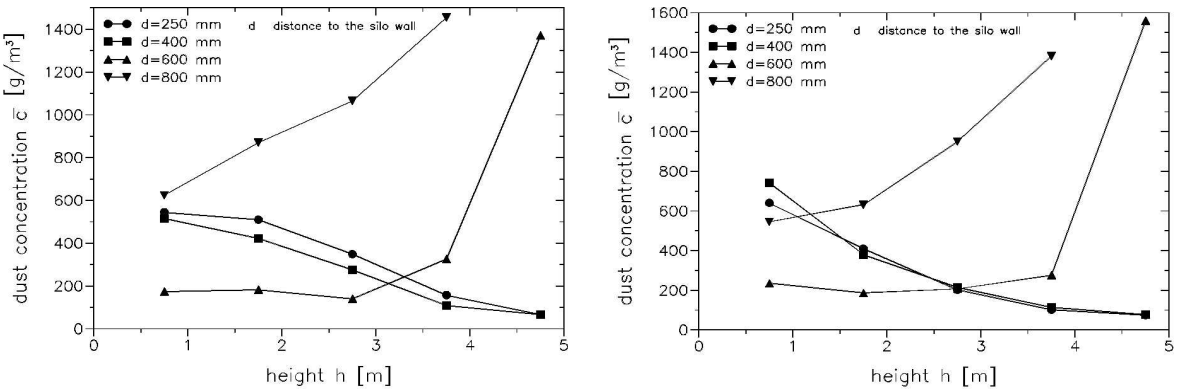

Figure 23: Mean dust concentration versus the height h at the silo fed vertical with a feeding rate of ξ=7 kg/m^3 (left picture) and ξ=7 kg/m^3 with dust in the hopper (right picture) using maize starch.

The results described so far refer to an empty vessel before it is filled, so that the dust is reflected at a bounce plate near the vessel outlet. Another series of measurements were carried out to investigate the effects upon the development of a dust cloud, when the conical part of the vessel is filled with dust. For comparison those results are shown in fig. 23 for a dust feeding rate of ξ = 7 kg/m^3. As can be seen the influence upon the measuring accuracy only refers to the lowest measuring point (h = 750 mm). Especially close to the wall (d = 250 or 400 mm) the dust concentration is strongly increasing.

Fig. 24 gives a survey of the results feeding the silo vertically (left side) and tangentially (right side) with a constant feeding rate of 7 kg/m^3.

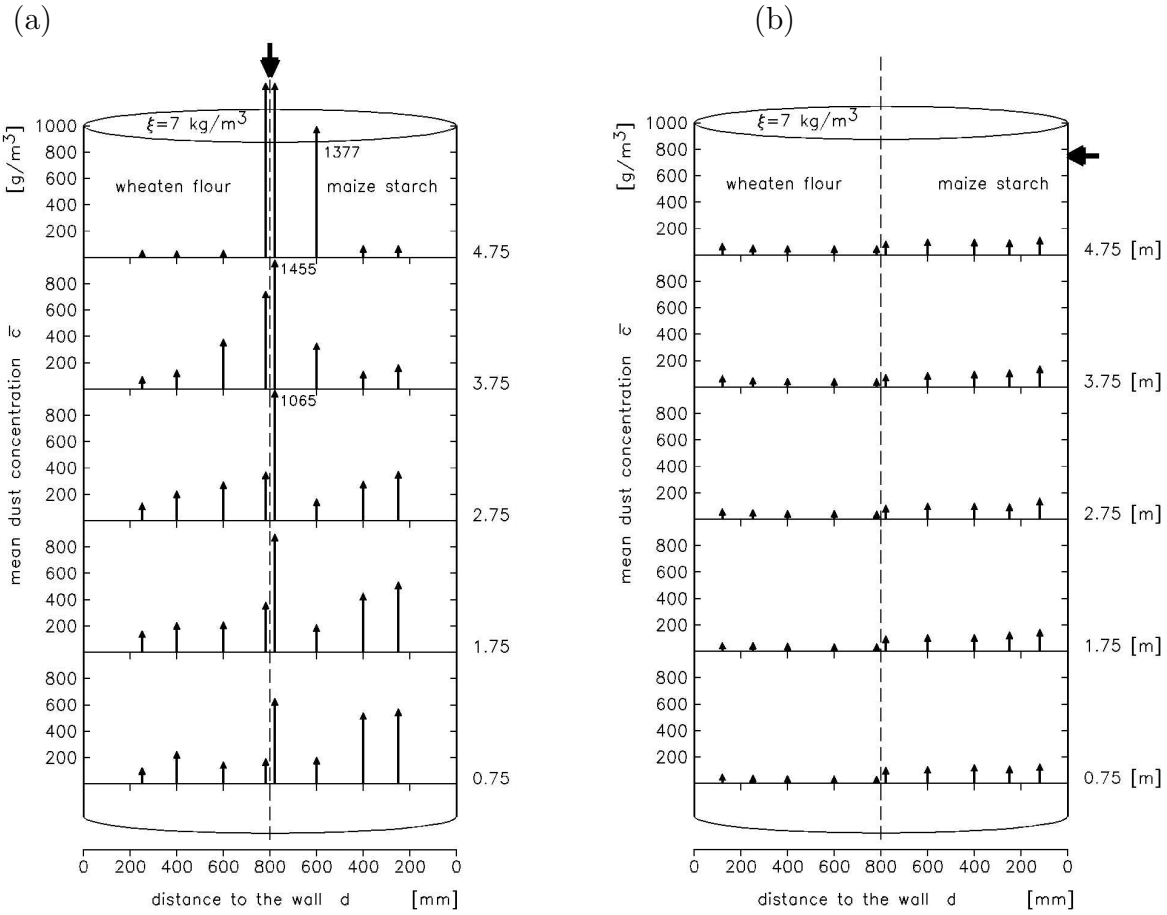

Figure 24: Distribution of the dust concentration (wheaten flour and maize starch) feeding the silo vertically (a) and (b) tangentially; feeding rate ξ=7 kg/m^3.

Tangential feeding

First, the silo was fed with maize starch and the feeding rate was varied. As shown in fig. 25 (a) and (b) the measured dust concentrations are quiet low $< 100\frac{g}{m^3}$ and nearly independent on the feeding rate within the range of 1 to 7 kg/m^3. Under the influence of the centrifugal forces the main part of the dust moves in a small layer around the inner surface of the silo and therefore, the measured concentration increases along the radial direction. The median value of wheaten flour and consequently the influence of the centrifugal forces is stronger compared with maize starch so that the dust concentration in the center of the silo is lower, that is $< 50\frac{g}{m^3}$.

When the dust close to the inner surface is not taken into consideration the dust distribution is nearly homogeneous and a low concentration was measured by feeding the silo tangentially. However, the dust concentration is higher but very inhomogeneous in the case of feeding the silo vertically.

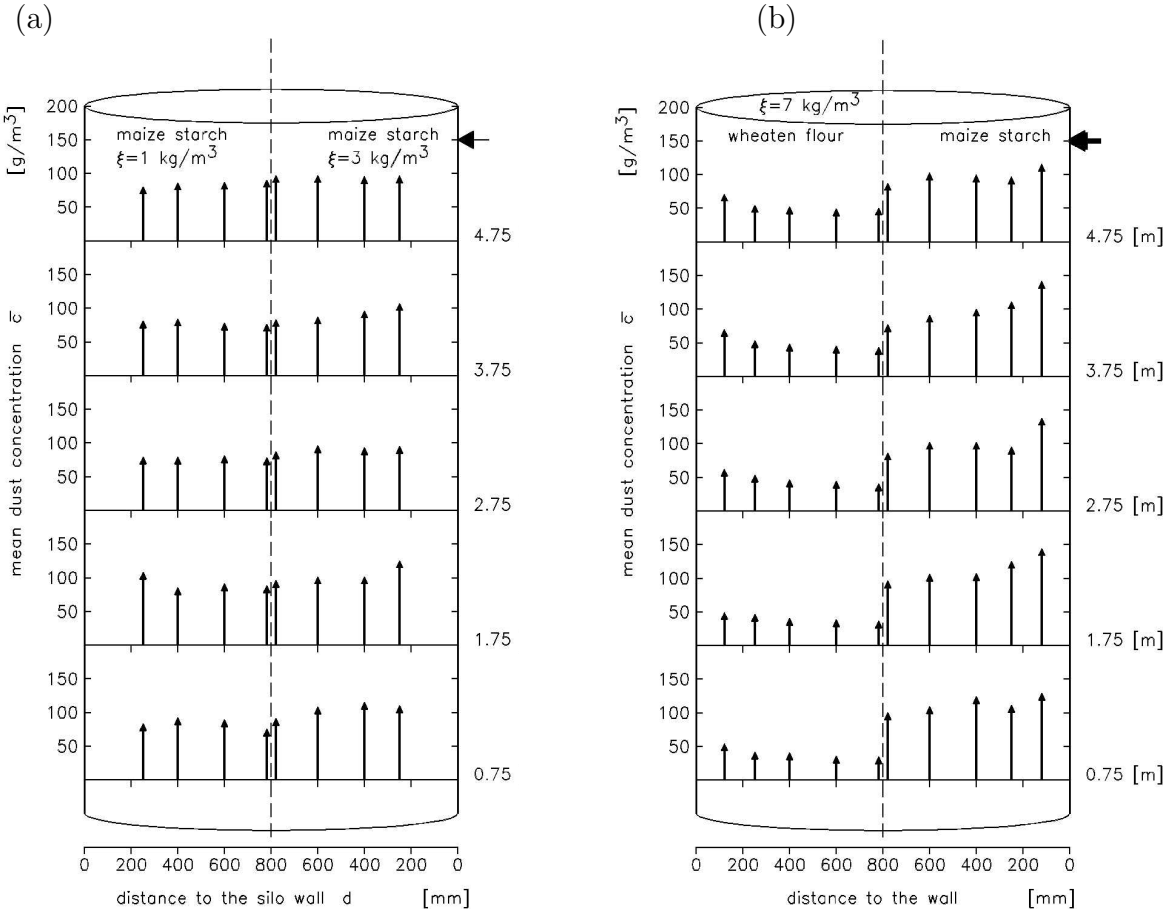

Figure 25: Distribution of the dust concentration feeding the silo tangential with (a) maize starch at feeding rates of 1 kg/m^3 and 3 kg/m^3 (b) maize starch and wheaten flour at a feeding rate of 7 kg/m^3.

Mechanical feeding

Finally, the silo was filled centrally by the means of a screw conveyor according fig. 9. The measured dust concentrations using a maximum quantity of 60 kg/min were in the same order as feeding the silo pneumatically with a feeding rate of 7 kg/m^3.

The gravitation and the force resulting from the horizontal velocity component of the conveyor force the dust particles on a parabolic trajectory pointed to the bottom of the silo.

The dust distribution is rather inhomogeneous as can be seen in fig. 26. In the conveying direction of the screw conveyor high local dust concentrations were determined; in the reversal direction the concentrations are quite low. Using wheaten flour we yield similar results, although the dust concentration close to the wall and near the surface of the deposited dust at the silo bottom is lower according to the larger particle size.

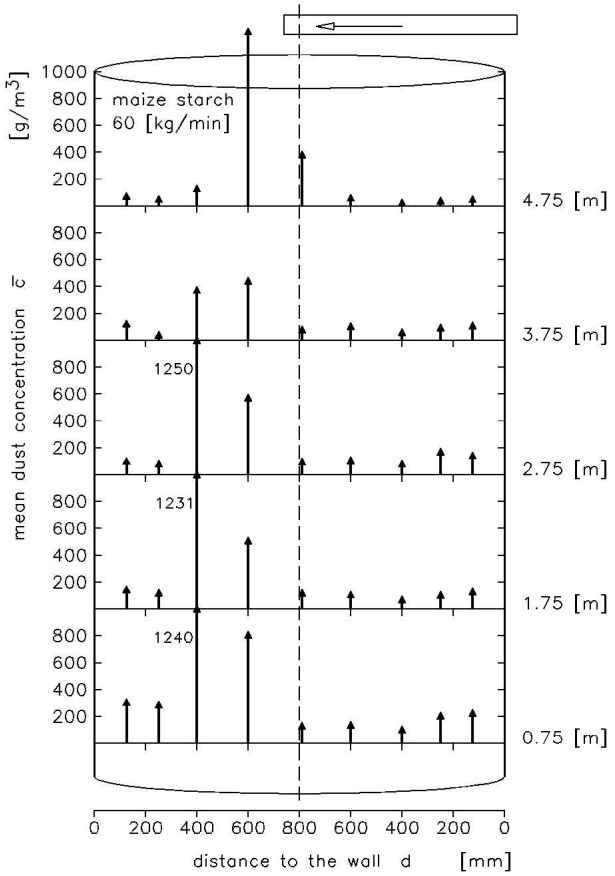

Figure 26: Distribution of the dust concentration in the mechanical fed silo using maize starch and rate of 60 kg/min.

4.3 Summary of the results

4.3.1 Turbulence

Vertical filling of the 12 m^3–Silo

- We found a rotary symmetry of the velocity of the dust particles.
- No dependence on the used type of dust neither on the velocity nor on the RMS turbulence velocity could be detected.
- Additionally a dependence on the feeding rate could not be determined.
- The highest RMS turbulence velocity we measured was in the order of 2.5 m/s.
- The maximum velocity is found in the center of the silo in z–direction. At the silo wall the particles will raise and the velocity reverses. Therefore, the turbulence has its maximum at the center of the beam.

Tangential filling of the 12 m^3–Silo

- The velocity of the tangential component decreases from the silo wall to the center of the silo in all planes.
- The corresponding RMS–turbulence velocity is nearly constant.

Mechanical filling of the 12 m^3–Silo

- The measured velocity of the particles was only about 0.25 m/s and the corresponding RMS turbulence velocity about 0.1 m/s.

4.3.2 Dust concentration

Vertical filling of the 12 m^3–Silo

- Close to the dust beam the concentration is rather high, as expected, but is decreasing to the silo wall.
- The concentration is decreasing to the silo wall for wheaten flour much more rapidly than for maize starch, due to the larger particle size.

Tangential filling of the 12 m^3–Silo

- The dust concentrations are quite low ($< 100\frac{g}{m^3}$) and nearly independent on the feeding rate within the range of 1 to 7 $\frac{kg}{m^3}$.

- Due to the influence of the centrifugal forces the main part of the dust immediately circulates around the wall of the silo, and therefore, the measured concentration increases towards the silo wall.
- Except from the dust layer near the wall the concentration is nearly homogeneous.

Mechanical filling of the 12 m^3–Silo

- The measured dust concentration is inhomogeneous and the amount is in the same order as pneumatical, vertical filling. The rotary symmetry is not satisfied.

5 Dust distribution in a crushing mill

Measurements were conducted at a new developed rotary grinding mill, where the expected dust concentration should be reduced in the hopper after the sieve. The various positions, where the dust concentration of barley dust was determined are shown in fig. 27.

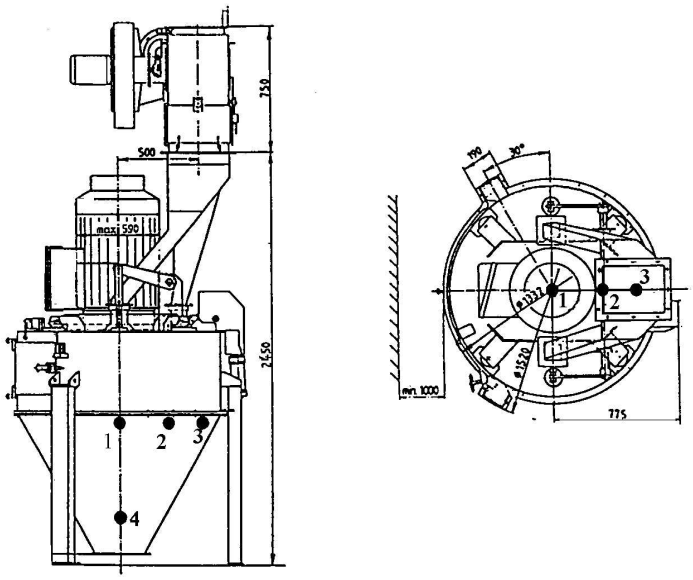

Figure 27: Schematic diagram of the crushing mill. Additionally the four positions to measure the dust concentration are shown.

5.1 Results

At every position the concentration of the ground barley dust was continuously measured during 60 seconds. Later the corresponding gauge measurement was carried out, with a sample of the dust. The following table shows the results of the measured dust concentration at the various positions.

Table 2: Dust concentration at the various positions in a grinding mill.

Position	mean concentration $\bar{c}$ $[\frac{g}{m^3}]$	max. concentration c_{max} $[\frac{g}{m^3}]$	min. concentration c_{min} $[\frac{g}{m^3}]$
1	60	100	30
2	100	150	70
3	170	230	120
4	240	380	150

Most of the dust is circulating close to the wall of the hopper due to the centrifugal force. Due to the geometry of the sensor probe it was not possible to measure closer than 120 mm to the wall of the hopper.

The finest–grinned barley is streaming essentially to the top of the hopper, while the rough particles fall down. Therefore, the dust concentration at position 4 is much higher compared with the other positions.

The lower explosion limit (LEL) of barley ($< 63\mu$m) is about 125 $\frac{g}{m^3}$.

6 Measurements at the standard 1 m^3–vessel

To compare measurements in process industries with those received in laboratory tests dust concentration and turbulence parameters were also determined at the standard 1 m^3–vessel [8].

The standard 1 m^3–vessel designed by ISO/VDI, is used in most dust explosion laboratories [9, 18]. Fig. 28 shows the schematic diagram and measuring system. The required quantity of dust is dispersed into the 1 m^3–vessel by an air flow from a pressurized bottle with an initial overpressure of 20 bar, which forces the dust in the dust chamber through a perforated ring nozzle according to ISO standard method. The measuring probes for the LDA–measurements were located at the center of the vessel (fig. 28), the probes for the dust measurement (DCM) at 9 different position in the vessel.

To avoid a fast soiling on the optical measuring probes in the 1 m^3–vessel we used maize starch concentrations between 30 g/m^3 and 120 g/m^3 for LDA measurements and 120 g/m^3 for measurements of the dust concentration.

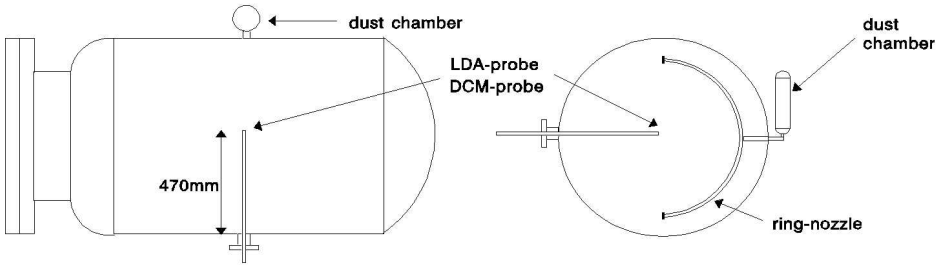

Figure 28: Schematic diagram of the 1 m^3–vessel and the location of the measuring system.

6.1 Dust Concentration

From the dust concentration measurements in the 1 m^3–vessel shown in fig. 29 one can observe that during the dispersion process the dust concentration increases at the first 300 ms and than decreases to about 200 g/m^3 at the ignition point after 600 ms. This time (0.6 s) is the standard delay time given in the ISO guideline [9].

The whole data set is shown in fig. 30, where the two data points at the center could not be determined exactly due to the soiling of the lenses.

6.2 Turbulence parameters

Fig. 31 demonstrates a typical instantaneous velocity profile for the horizontal component in the 1 m^3–vessel, where it is shown that the dispersion process is strongly time dependent. Five independent single measurements were averaged in a time interval, where the length of the time interval was determined empirically. The figure gives also the RMS turbulence velocity as a function of the time. The decay was first fitted with the function

$$y = a \cdot e^{-b \cdot t} + c\,.$$

As can be seen at 600 ms the RMS turbulence velocity is decreased to 1.2 m/s.

Fig. 32 demonstrates that the maximum measured mean velocities for the *vertical* component at the center in the standard 1 m^3–vessel is much higher than for the horizontal component due to the arrangement of the drilling in the ring nozzle. The RMS turbulent velocity reaches a value at 600 ms of 2.64 m/s.

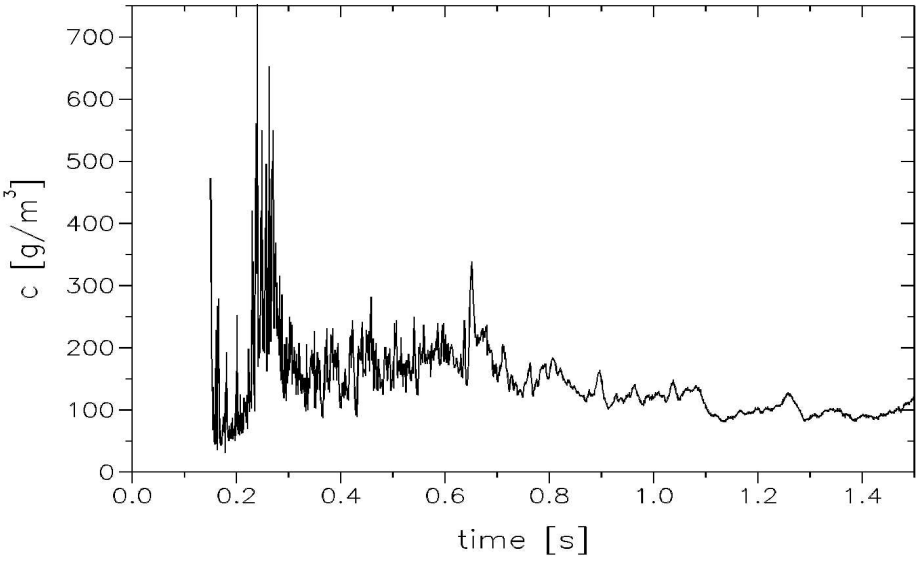

Figure 29: Dust concentration during the dispersion process in the 1 m^3–vessel as a function of time. The optic transducer was opened at t=0.15 s. The DCM–probe was located at the center of the vessel.

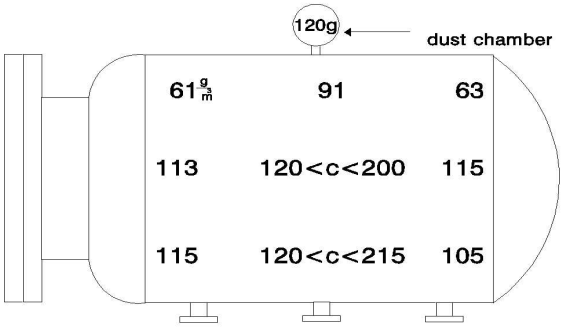

Figure 30: The dust concentration at 9 various positions in the standard 1 m^3–vessel in the unit $\frac{g}{m^3}$. The initial amount of dust in the dust chamber was 120 g. The results of one single time course were averaged, just as the results of various measurements.

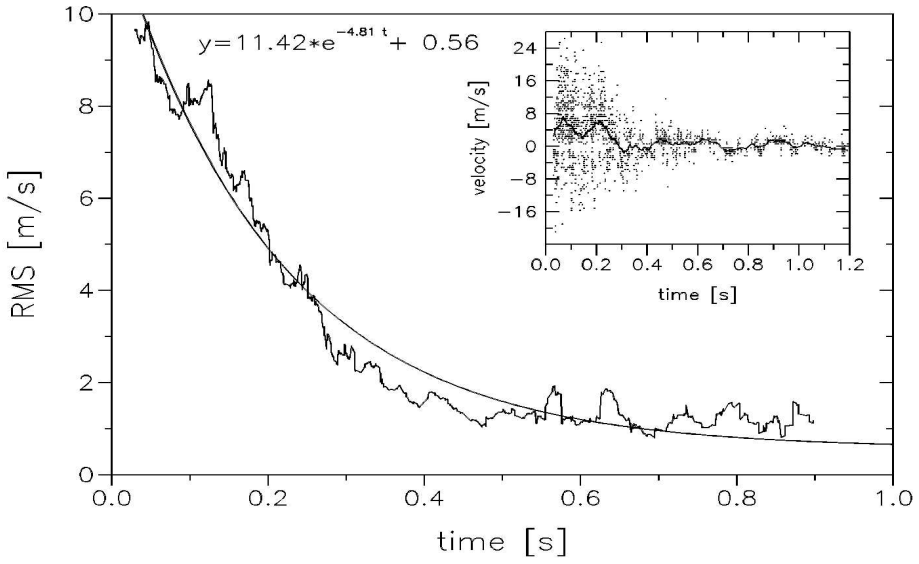

Figure 31: RMS turbulence velocity (horizontal component) as a function of the time at the center of the 1 m^3–vessel with the regression curve according to $y = a \cdot e^{-b \cdot t} + c$. The inset shows the typical instantaneous horizontal component of the flow velocities as a function of the time.

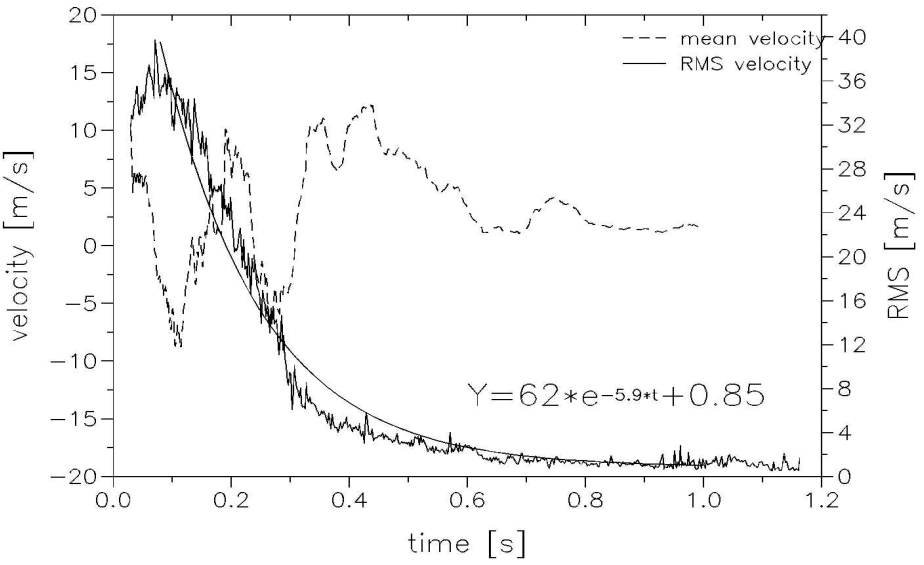

Figure 32: RMS turbulence velocity (vertical component) as a function of the time at the center of the 1 m^3–vessel with the regression curve according to $y = a \cdot e^{-b \cdot t} + c$.

7 Fluidized bed drier

Dust concentration measurements were carried out in the fluidized bed of a drier, where the complete system is shown schematically in fig. 33.

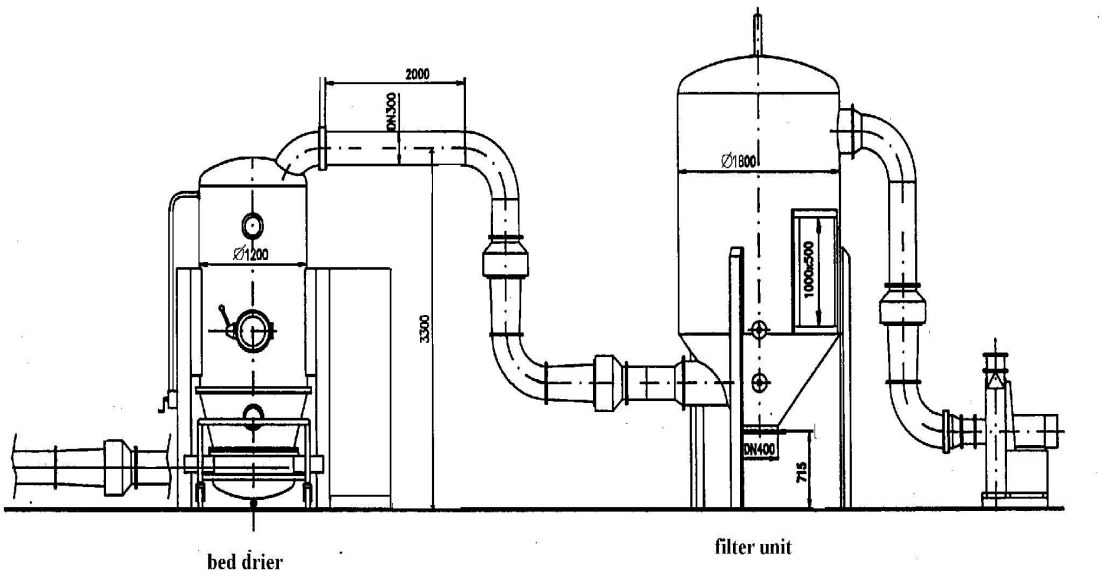

Figure 33: Schematic diagram of the fluidized bed drier and the filter unit. Volume of the drier V= 3.2 m^3, Volume of the filter V= 7.1 m^3.

The dust concentration measuring probe was located 1100 mm above the sieve plate, that is about 750 mm above the surface of the dust layer. Fig. 34 shows the influence of the amount of dust in the chamber and the volume flow.

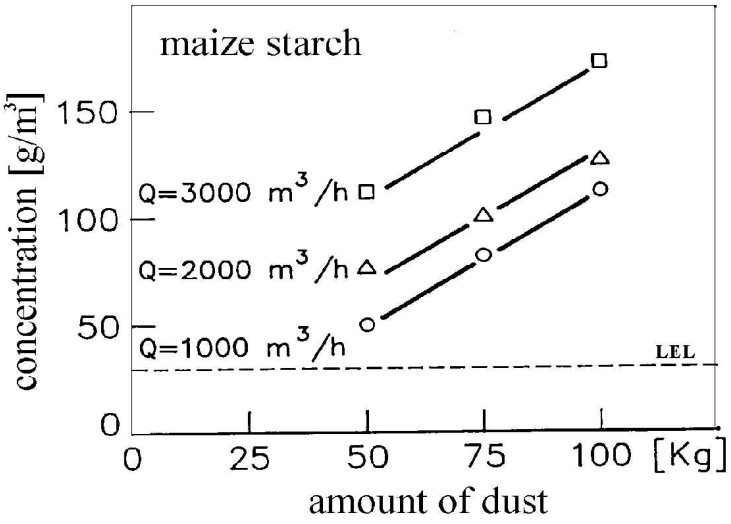

Figure 34: Dust concentration as a function of the amount of product (maize starch) in the chamber of a fluidized bed drier for three different volume flows.

It can be seen that the dust concentration increases linear with growing amount of dust and that the concentration exceeds always the lower explosion limit.

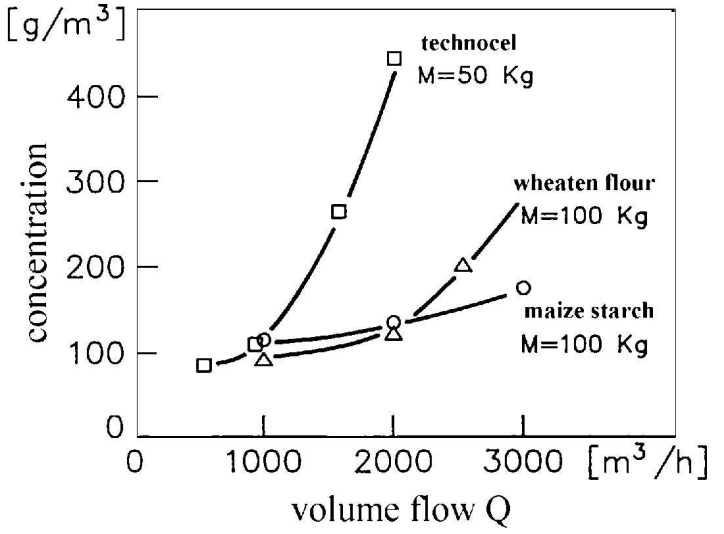

Figure 35: Measured dust concentration as a function of the volume flow in a fluidized bed drier for three dust types.

When the probe was located 800 mm above the sieve plate, the concentration was strongly increasing but did not exceed the UEL. Therefore, it can be demonstrated, that the dust distribution in the fluidized bed drier is, as expected, inhomogeneous but within the explosion limits.

In a second step the influence of the volume flow using a constant amount of dust was investigated. Fig. 35 shows the results, where up to 1000 $\frac{m^3}{h}$ no influence of the type of dust was found, when the probe was located 1100 mm above the sieve plate.

7.1 Filter unit

In further investigations the exhaust air of the bed drier was cleaned in a subsequent filter unit (fig. 33). Measurements of the dust concentration in the tube connecting the bed drier and the filter showed that – choosing the right filter element – the LEL was never exceeded.

Due to an occasional occurring tear in the filter insert in the drier, the dust concentration in the tube is increasing and exceeds the lower explosion limit. Turbulence measurements in tubes of such pneumatic systems are described in chapter 11.

Such concentrations were also measured directly behind the inlet of the filter unit (110 mm above the bottom of the filter), which is shown in fig. 36 as a function of the volume air flow for different types of dust. It is also shown, that the dust concentration decreases rapidly, if the measuring position is moved to the top of the filter.

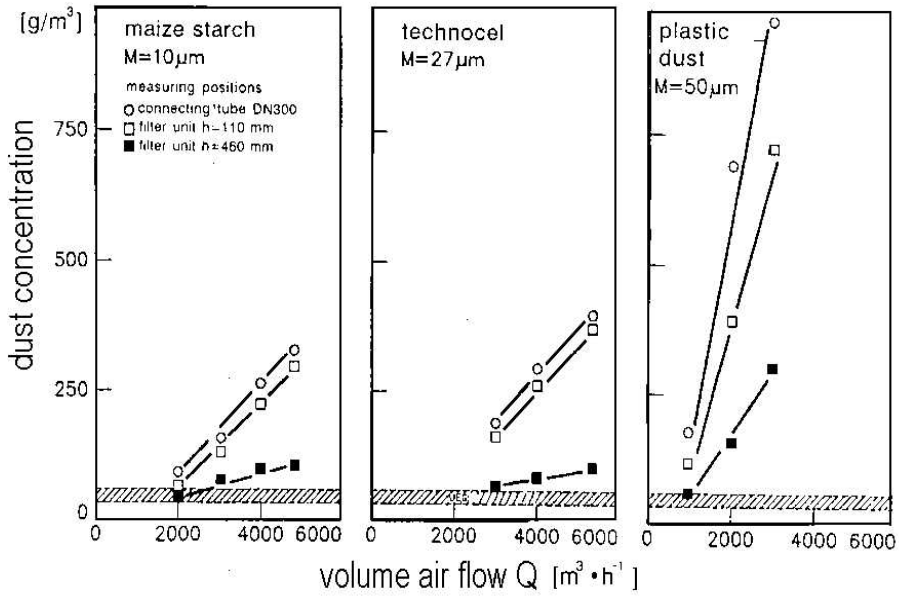

Figure 36: Measured dust concentration in the filter unit for three types of dust as a function of the volume air flow. Additionally the LEL is marked in the diagram.

8 Measurements in a filter unit for wood dust

This filter unit is often used to suck off dust from machines especially in the timber industry. With an area of the filter material of 22 m^2 the maximum filter efficiency is limited up to 2500 m^3/h. The exhaust air reaches the filter unit through a diffusor, which reduces the velocity of the conveying flow. Fig. 37 gives a survey of the complete filter system and fig. 38 shows the location of the dust concentration measuring probe below the filter tubes.

The filter tubes are cleaned pneumatically, where the frequency of the pressure air blasts (duration 1s) could be adjusted between 5 and 90 minutes. The deposited dust or the shavings at the bottom can be sucked off by the means of a tube.

Figure 37: Survey of the complete filter system. The inset shows the positions of the dust concentration measuring probes, which were located below the diffusor and below the filter tubes, respectively.

Fig. 39-40 show the measured dust concentration as a function of the rate of dust flow. The location of the probes and the use of a cleaning system was also varied. The wood dust (beech) has a median value of 75 μm.

As can be seen in the diagrams the LEL of 60 g/m^3 was never exceeded without cleaning the filter tubes. Even in practice the amount of wood dust cannot exceed $\approx$ 350 g/min concerning this type of filter. The concentration is increasing, cleaning the filter tubes pneumatically (see the dotted lines in fig. 39–40).

Figure 38: Location of the dust concentration measuring probe (arrow) below the filter tubes .

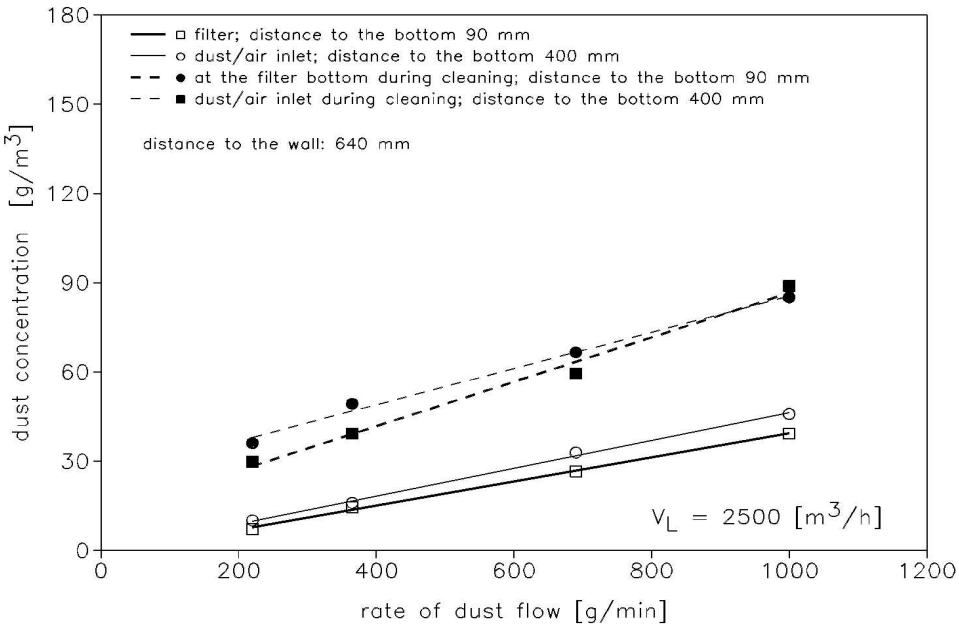

Figure 39: Dust concentration in a filter unit for wood dust vs. rate of dust flow at different positions of the probe. *The suction unit was switched off*; distance of the probe to the wall: 640 mm. The dotted lines show the results during the cleaning of the filter tubes.

Further investigations demonstrated, that the cleaning system is more effective, when the suction unit is working, because a larger amount of dust could be blown off from the filter tubes. This situation is shown in fig. 40. The measured peaks in concentration are nearly independent of the amount of dust, but dependent of the soiling of the filter tubes.

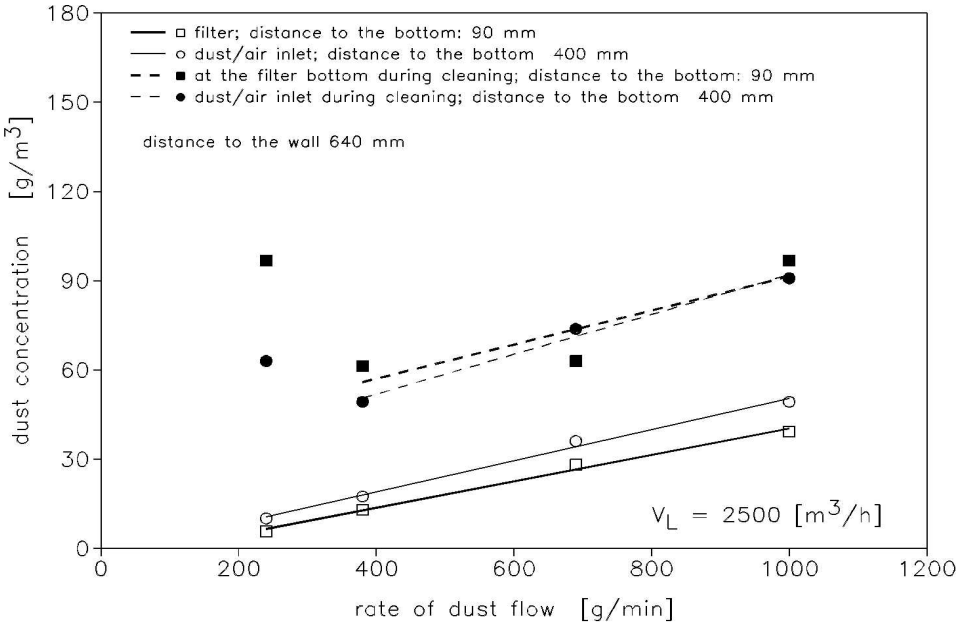

Figure 40: Dust concentration in a filter unit for wood dust vs. rate of dust flow at different positions of the probe. *The suction unit was switched on*; distance of the probe to the wall: 640 mm. The dotted lines show the results during the cleaning of the filter tubes.

In summary it may be said, that the lower explosion limit is only exceeded in some partial areas of the filter unit for a short duration of a few seconds, when the tube cleaning system is active.

9 Measurements in a discharge trench[1]

The measurements were conducted at a discharge trench of an animal food manufacturer [22], with the dimension of 23 m (length)× 6 m (width) × 2.4 m (depth).

For ventilation a suction unit with a capacity of 60000 m^3/h had been installed along the length of the trench.

The generation of dust clouds during the discharge and unloading of trucks at such a trench is hard to predict. The size and the density of the dust clouds depend upon many parameters, such as

- characteristics of the type of dust (e.g. amount of fine particles, moisture content)
- means of unloading of the trucks (e.g. discharge from the side, discharge through the hopper of the silo, use of containers with conveyor bottom)
- discharge height
- size of the discharge trench
- soiling of the trench by previously unloaded dust
- efficiency of a ventilation/suction system

In order to measure extreme conditions, the discharge system of a special transporter was manipulated in such a way, that intensive dust cloud generation was obtained. The subject special transporter was a container type unit in which a wall pushes the dust towards the outlet. In order to create larger dust clouds the outlet was closed and the door at the end of the container was opened. Therefore, a larger mass of bulk product was dropped into the discharge trench.

The bulk product transported by this special transporter unit was "Maisarin". Maisarin is an animal foodstuff resulting from processing of maize starch with a particle size distribution of 30% < 250 μm and 7% < 63 μm. The moisture content of the dust was 10.6%. The measuring position was located at the most critical location just above the edge of the discharge trench. Fig. 41 shows the experimental set up.

Fig.42 shows a typical result of the measured dust concentration. In order to obtain an indication regarding the possible hazards a laboratory test was done to determine the lower explosion limit (LEL) of Maisarin. The LEL of 60 g/m^3 as obtained from tests in the 20 l -sphere is also shown in fig. 42.

During the measurements the LEL of the discharged product has been exceeded 10 times for a period of 1 up to 5 seconds during the unloading process (total discharge time 15,5 min). The occurrence of combustible dust/air mixtures outside

[1]Experiments were carried out by C. Zockoll

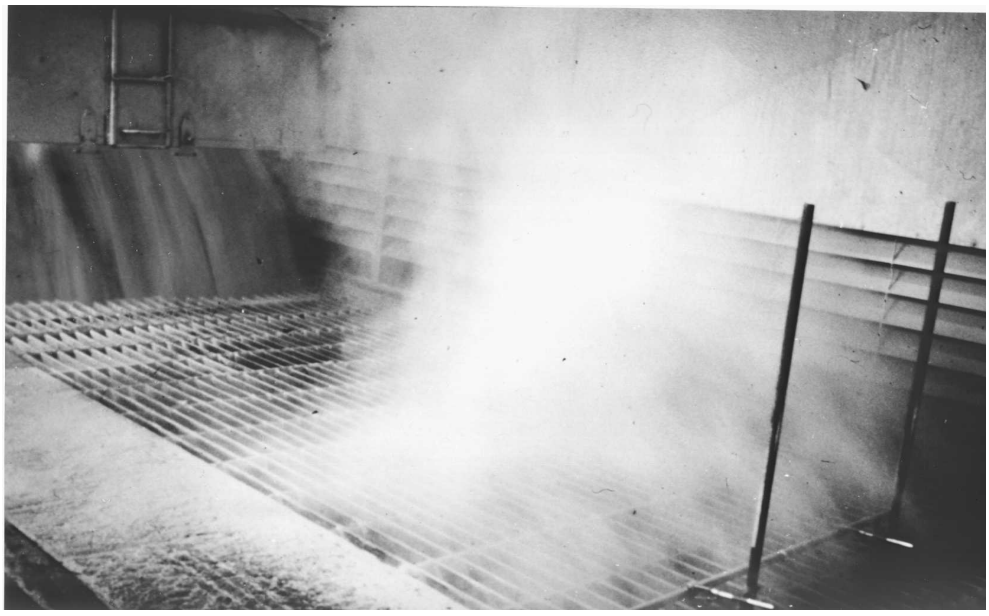

Figure 41: Measurement of dust concentration (Maisarin) at the discharge trench [22].

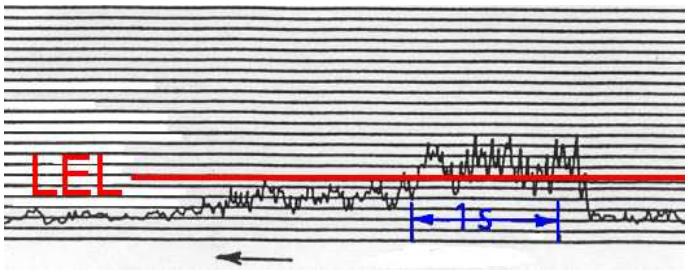

Figure 42: Typical time history of dust concentration measured in a discharge trench.

the discharge trench is not expected due to the discharging with the normal outlet of the transporter.

Unloading 15 tons of Maisarin by dumping the load sideways the largest suspended dust cloud during the tests at the discharge trench has been measured. During this discharge of the dust the LEL has been exceeded during 8 subsequent seconds without interruption. The total measured time, during which the LEL was exceeded, was 27 seconds. When similar experiments were carried out using other dusts such as wheaten bran barley, toasted soya beans and other discharge processes, respectively, (for example silo-type trucks with floor-discharge) the LEL was exceeded only during very short durations.

10 Measurements in ship hulls[1]

The discharge process in ship hulls was investigated [22] with two different dust types, considered to be very critical: maizegluten and tapioca. The discharge of maizegluten (maizegluten pellets with dust content 4.5% < 63 μm moisture content 8.6%) was conducted by means of a crane. Inside the ship a bulldozer was used to assist in providing the bulk material towards the crane area. The ship hull had following dimensions: length 28 m, width 24 m and depth 12.5 m. During the measurements the working area was located at approximately 8 m.

For another dust namely tapioca the influence of a pneumatic conveyor and a mechanical unloading system were investigated. The ship hull had following dimensions: length 33 m, width 24 m and depth 12 m. During the measurements the working area was located at approximately 9 m. In order to assure the registration of the largest dust generations, the measurements were mainly carried out at the immediate surroundings of the discharge installations.

The LEL was exceeded during approx. 2 seconds as can be seen in fig. 43. Fig. 44 illustrates the effects and size of the dust cloud, which was generated. The measuring position was located at the forward tip of the probe. During the total measured time lap of approx. 440 seconds two individual situations were found at which the measured dust concentration exceeds the safety limits; additional to the description above, after approximately 2 seconds another period of approximately 0.13 seconds was observed.

Fig. 45 illustrates the conditions during the unloading process of tapioca (tapioca pellets, 11.2% < 63 μm, moisture content 9.7%). The LEL of tapioca dust has a amount of 40 $\frac{g}{m^3}$. Fig. 46 shows the corresponding time course. The LEL was never exceeded. During the total measurements the LEL (determined in laboratory tests) was only exceeded twice for a time period of less than 0.1 seconds.

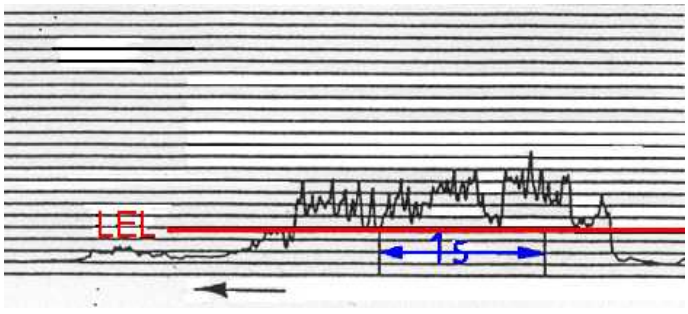

Figure 43: Dust concentration vs. time for maizegluten moved with a bulldozer in a ship hull [22].

[1]Experiments were carried out by C. Zockoll

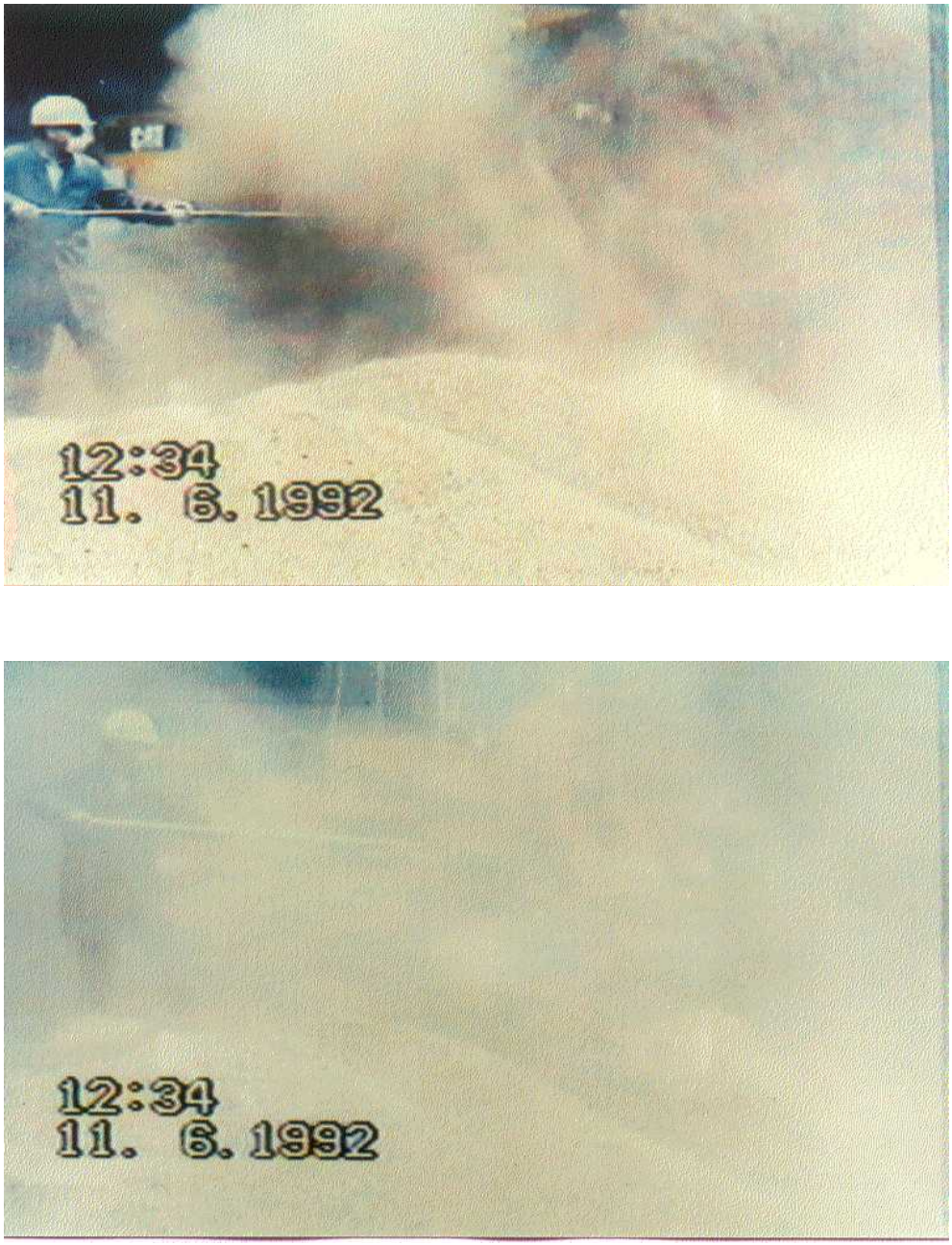

Figure 44: Generation of a dust cloud of maizegluten in a ship hull. The highest concentration is shown in the lower picture. The corresponding time course of the concentration is shown in fig. 43.

Figure 45: Dust concentration during the unloading of tapioca in a ship hull using a mechanical unloading system.

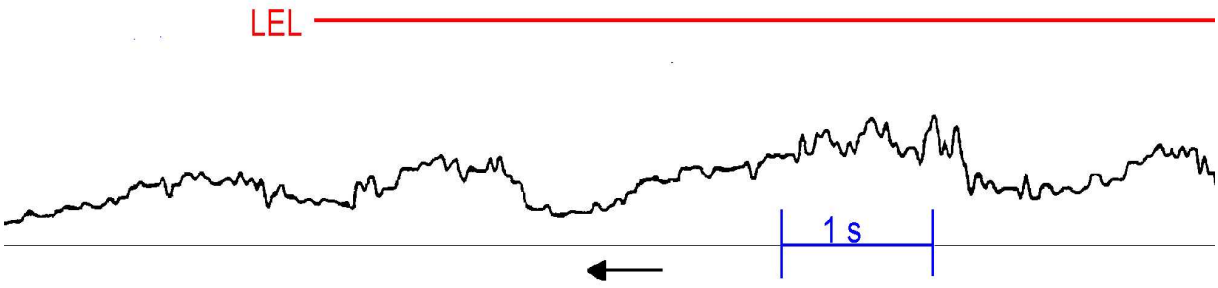

Figure 46: Time course of the dust concentration time course corresponding to fig. 45.

10.1 Discussion of the measured results

Those measurements indicate, that the periods exceeding the LEL are relatively short with the given discharge technologies [22]. The optical impression, that the dust clouds as generated during such discontinuous unloading processes will result in large combustible volumes are misleading. The volume of the suspended dust clouds extends fast, where the rough particles will deposit first. Due to the expanding of the volume the dust concentration is rapidly reduced and the LEL will be exceeded no longer. If the volume of the area is to small, the concentration of the suspended dust in the cloud will increase. Whether the LEL is exceeded in this event, depends upon the emitted amount of dust, the characteristics of the dust (e.g. particle size distribution, moisture content, aerodynamic behavior) and the air flow conditions.

Outside the discharge trench the increase of the dust cloud volume was reduced by the ventilation system. Directly at the measuring position, however, no visible effect of this equipment was found. However, the presented results will not enable us to describe the characteristics and propagation of dust clouds completely. Providing unfavorable conditions and location of the measuring device as close as possible to the emission source, respectively, such experiments will generate a realistic assessment of the hazard.

11 Turbulence measurements in a tube

For the experimental investigations a pneumatic conveying system was used consisting of a dust feeder, a conveying pipe, a cyclone and a suction fan to establish the air flow. The principle pictures of the test set is illustrated in fig. 47.

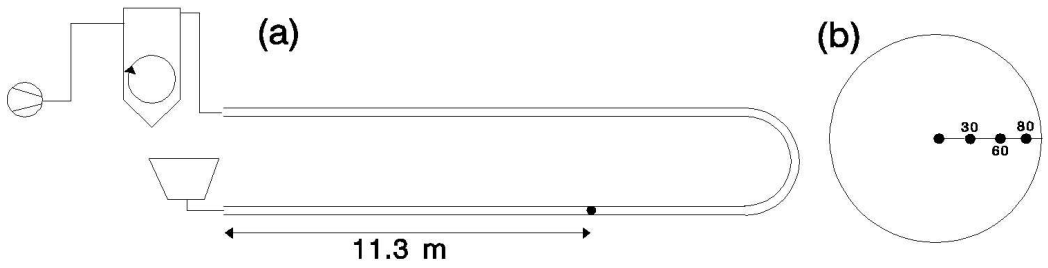

Figure 47: (a) Pneumatic conveying system for measurements of the eddy flow in the tube. (b) shows the four positions, where the measurements were conducted. They are located at 0 mm, 30 mm, 60 mm and 80 mm distance to the center.

The air was sucked into the system through the totally open tube at the dust feeding point by the underpressure generated by the suction. The dust concentration was

about 30 g/m^3. The turbulence and velocity measurements were conducted in a tube with a diameter of 200 mm.

Fig. 48 shows the influence of the various mean conveying velocities on the shape of the flow. The vertical bars shows the averaged RMS turbulence velocities.

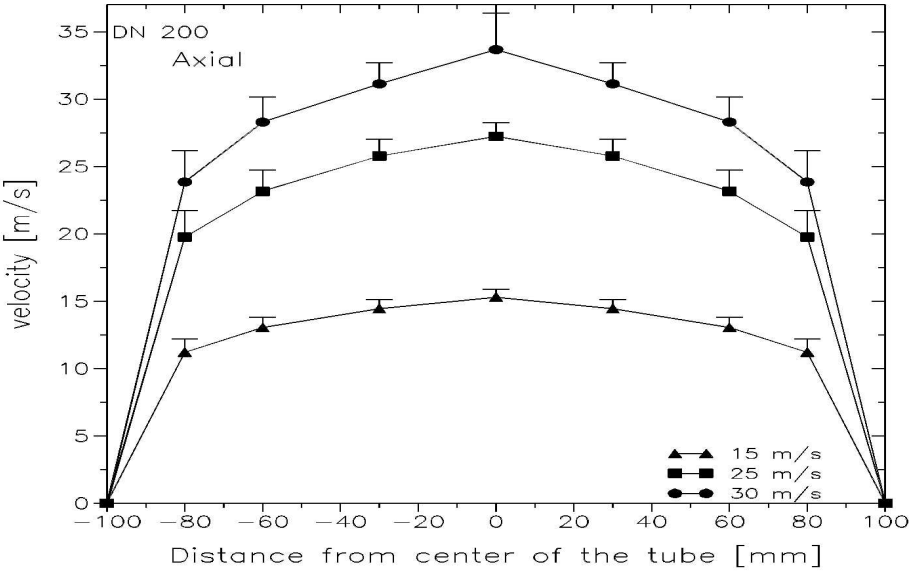

Figure 48: Measured velocities and the corresponding RMS turbulence velocities (illustrated as bars) vs. the cross-section of the tube using mean conveying velocities from 15 to 30 m/s.

Single values of the RMS turbulence velocities up to 8 m/s (!) were measured at different moments, which shows the rather high turbulence in tubes. Explosion tests in this system were also carried out by Vogl [19].

The three dimensional view of the profile of the flow is shown in fig. 49.

Fig. 50 shows the average axial RMS turbulence velocity across the cross-section of the tube for the three different conveying velocities. The linear proportionality is expected according to the Reynolds number.

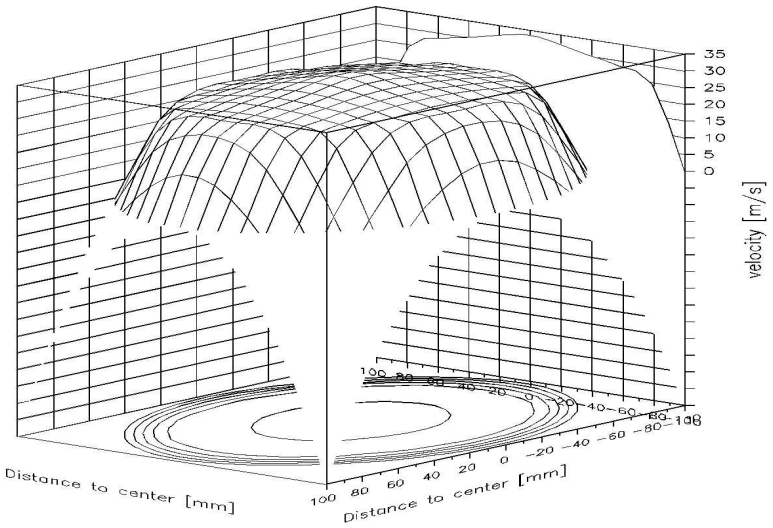

Figure 49: Three dimensional view of the eddy flow in a tube with a diameter of 200 mm.

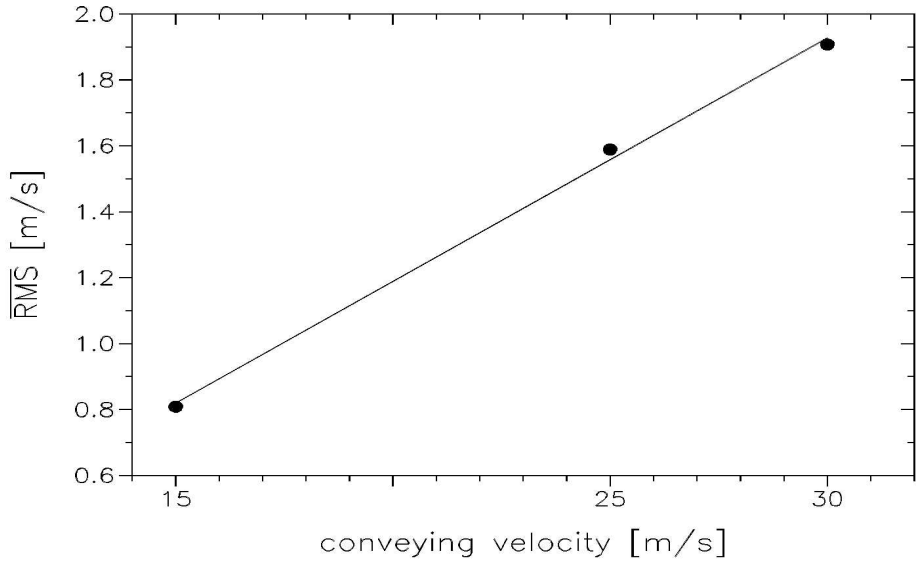

Figure 50: Axial RMS turbulence velocity averaged across the cross-section of the tube as a function of the conveying velocity.

References

[1] Amyotte P.R., Chippett S., Pegg M.J. Effects of Turbulence on Dust Explosion. *Prog.Energy Combust.*, 14:293–310, Dezember 1988.

[2] Armbruster L., Breuer H., Neulinger G. Photometric Dertermination of Respirable Dust Concentration without Elutriation of Coarse Particles. *Particle Characterization*, 1:96–101, 1984.

[3] Bartknecht W. *Explosionsschutz*. Springer–Verlag, 2. edition, 1993.

[4] Christill M., Nastoll W., Leuckel W., Zarzalis N. Der Einfluß von Strömungsturbulenz auf den Explosionsablauf in Staub/Luft-Gemischen. In VDI Berichte 701, *Sichere Handhabung brennbarer Stäube*, pages 123–141. VDI—Verlag, Düsseldorf, 1988.

[5] Durst F., Melling A., Whitelaw J.H. *Priciples and Practice of Laser–Doppler –Anemometrie*. Academic Press, London, 1981.

[6] Eckhoff R.K. *Dust explosions in the process industries*. Butterworth-Heinemann, 1991.

[7] Eckhoff R.K. Influence of Initial and Explosions-Induced Turbulence on Dust Explosions in Closed and Vented Vessels, Research on CMI. *Powder Technology*, 71:181–187, 1992.

[8] Hauert F., Vogl A., Radandt S. Measurement of Turbulence and Dust Concentration in Silos and Vessels. In *Proceedings of 6th International Colloquium on Dust Explosions*, pages 71–80, Shenyang, China, 1994.

[9] ISO 6184/1. Explosion Protection Systems: Determination of Explosition Indices of Combustible Dust in Air. Technical Report Part 1, International Organization for Standardardization, 1985.

[10] Hinze J.O. *Turbulence*. McGraw-Hill, 1959.

[11] Kauffman C.W., Srinath S.R., Tezok F.I., Nicholls J.A., Sichel M. Turbulent and Accelerating Dust Flames. In *Twentieth Symposium on Combustion*, pages 1701–1708. The Combustion Institute, 1984.

[12] Leidinger G., Schmalfuss H. Theoretische Überlegungen zur praxisgerechten In–situ– Streulichtmessung von Ruß und Staub. *Staub–Reinhaltung der Luft*, 53:193–199, 1993.

[13] Pu Y.K., Jarosinski J., Johnson V.G., Kauffman C.W. Turbulence effects on dust explosions in the 20-liter spherical vessel. In *Twenty–Third Symposium on Combustion*, pages 843–849. The Combustion Institute, 1990.

[14] Ruck B. *Laser–Doppler–Anemometrie*. AT-Fachverlag, Stuttgart, 1987.

[15] Ruck B. Einfluß der Tracerteilchengröße auf die Signalinformationen in der Laser–Doppler–Anemometrie (Influence of Tracer Particle Size on Flow Information in LDA). *Technisches Messen*, 57(7/8):284–295, 1990.

[16] Scheuermann K., Klug M., Bielert U., Adomeit G. Zum Einfluß der Turbulenz auf den Explosionsablauf. In VDI Berichte 975, *Sichere Handhabung brennbarer Stäube*, pages 253–271. VDI—Verlag, Düsseldorf, 1992.

[17] Schledde R. Ein neues Glasfaser–Laser–Doppler–Anemometer zur Strömungs– und Oberflächengeschwindigkeitsmessung. In *Laser Jahrbuch*. Vulkan–Verlag, Essen, 2.Ausgabe.

[18] VDI 2263. Dust fires and dust explosions. Technical report, Verein deutscher Ingenieure,(VDI), 1992.

[19] Vogl A. The Course of Dust Explosions in Pipes and Pneumatic Systems. In *Proceedings of 6th International Colloquium on Dust Explosions*, pages 535–552, Shenyang, China, 1994.

[20] Vogl A., Ott H., Hauert F. Handbuch zum Staubkonzentrationsmeßgerät SKG5. Technical report, Forschungsgesellschaft für angewandte Systemsicherheit und Arbeitsmedizin, Mannheim, 1993.

[21] Walcher H. Die fotoelektrische Messung von Staubemissionen. *Feinwerktechnik*, 83(6):257–262, 1975.

[22] Zockoll C. Concentration and Ignitability of Dust Clouds during the Discharge of Bulk Material. In *Proceedings of 6th International Colloquium on Dust Explosions*, pages 263–277, Shenyang, China, 1994.